VISION-BASED CLASSIFICATION OF SOLDER JOINT DEFECTS

NANG SENG SIRI MAR

SUBMITTED AS A REQUIREMENT FOR
THE DEGREE OF

MASTER OF ENGINEERING (RESEARCH)

AT THE

SCHOOL OF ENGINEERING SYSTEMS

FACULTY OF BUILT ENVIRONMENT AND ENGINEERING

QUEENSLAND UNIVERSITY OF TECHNOLOGY

BRISBANE, AUSTRALIA

APRIL, 2010

Keywords

Automatic PCB inspection, Segmentation of solder joint, Illumination normalisation, Gabor filter, Log Gabor filter, Discrete Wavelet Transform, Discrete Cosine Transform, Mahalanobis Cosine Distance, Classifier fusion,

Abstract

Inspection of solder joints has been a critical process in the electronic manufacturing industry to reduce manufacturing cost, improve yield, and ensure product quality and reliability. The solder joint inspection problem is more challenging than many other visual inspections because of the variability in the appearance of solder joints. Although many research works and various techniques have been developed to classify defect in solder joints, these methods have complex systems of illumination for image acquisition and complicated classification algorithms. An important stage of the analysis is to select the right method for the classification. Better inspection technologies are needed to fill the gap between available inspection capabilities and industry systems.

This dissertation aims to provide a solution that can overcome some of the limitations of current inspection techniques. This research proposes two inspection steps for automatic solder joint classification system. The “front-end” inspection system includes illumination normalisation, localization and segmentation. The illumination normalisation approach can effectively and efficiently eliminate the effect of uneven illumination while keeping the properties of the processed image.

The “back-end” inspection involves the classification of solder joints by using Log Gabor filter and classifier fusion. Five different levels of solder quality with respect to the amount of solder paste have been defined. Log Gabor filter has been demonstrated to achieve high recognition rates and is resistant to misalignment. Further testing demonstrates the advantage of Log Gabor filter over both Discrete Wavelet Transform and Discrete Cosine Transform. Classifier score fusion is analysed for improving recognition rate. Experimental results demonstrate that the proposed system improves performance and robustness in terms of classification rates. This proposed system does not need any special illumination system, and the images are acquired by an ordinary digital camera. In fact, the choice of suitable features allows one to overcome the problem given by the use of non complex illumination systems. The new system proposed in this research can be

incorporated in the development of an automated non-contact, non-destructive and low cost solder joint quality inspection system.

Contents

List of Tables

List of Figures

List of Abbreviations

PCB	Printed Circuit Board
IC	Integrated Circuits
AOI	Automatic Optical Inspection
DCT	Discrete Cosine Transform
DWT	Discrete Wavelet Transform
ROI	Region Of Interest
RGB	Red, Green, Blue
YIQ	Luminance, In-phase, Quadrature
DET	Detection Error Trade-off
SMT	Surface Mount Technology
LED	Light Emitting Diode
ANN	Artificial Neural Network
LVQ	Learning Vector Quantisation
EER	Equal Error Rate
FFT	Fast Fourier Transform
llr	linear logistic regression

List of Symbols

ρ	orientation of the line
θ	distance to the origin
x	horizontal coordinate in the image space
y	vertical coordinate in the image space
$M \times N$	matrix associated with the normalised image
$D(x,y)$	2d – Discrete Cosine Transform
α	intensity of the pixels
$f(x,y)$	2d – Inverse Discrete Cosine transform
C_{uv}	coefficients in Discrete Cosine transform
Y	luminance
I	in-phase
Q	quadrature
R	red
G	green
B	blue
A	a set
B	symmetric structuring element
k	number of iteration
X_k	a value calculate for k iteration step
H	horizontal projection
V	vertical projection
λ	i^{th} row of the thresholded image
γ	j^{th} column of the thresholded image
s	complex sinusoidal carrier
ω_r	Gaussian envelop
u_0	spatial frequency of the sinusoidal (x- coordinate)
v_0	spatial frequency of the sinusoidal (y- coordinate)

g	Gaussian filter
a	sharpness of the Gaussian envelope (x- coordinate)
b	sharpness of the Gaussian envelope (y- coordinate)
φ	rotation of the Gaussian about the origin
Φ	frequency response of Log-Gabor filter
ω_0	center frequency of the sinusoid
Ψ	Haar wavelet transform
t	time
$\vec{x}$	2D DCT feature vector
σ	standard deviation
$D_{Mahcosine}$	Mahalanobis cosine distance
θ_{mn}	angle between m and n image
C_k	k^{th} classifier
β_k	the weigh given to the k^{th} classifier
C_{weight_sum}	weight fusion
P	synthetic prior
K	number of true trial
L	number of false trial
C_{llr}	cost function of linear logistic regression
f_j	fused target scores
g_j	non-target scores
s_{ij} , r_{ij}	detection trials
χ	constant value for detection trials

Authorship

The work contained in this thesis has not been previously submitted for a degree or diploma at any other higher education institution. To the best of my knowledge and belief, the thesis contains no material previously published or written by another person except where due reference is made.

Signed: _____

Date: _____

Acknowledgements

Though it is a single name that is attributed as author of this work, there are many people without whom it could never been completed. Firstly, I thank my parents who encouraged me to enter the Master program and who have supported me throughout my studies. I would like to thank my principal supervisor Professor Prasad Yarlagadda and my associate supervisor Dr. Clinton Fookes. In particular I must acknowledge the members of the MRD Rail Technologies especially Sathish who helped me to get the Printed Circuit Board for my project. I would also like to extend a big thank you to Queensland University of Technology, which creates a colourful and creative environment to complete my studies. There are many others who helped me throughout my time here in the lab and to you all I extend a big thank you for your friendship and support.

Publications Resulting from this Thesis

Listed below are the peer-reviewed publications resulting from this research programme.

Journal Articles

N. S. S. Mar, C. Fookes and P. K. D.V. Yarlagadda, “Design of Automatic Vision-based Inspection System for Solder Joint Segmentation,” Achievements in Materials and Manufacturing Engineering, pp.145-151, 2009.

N. S. S. Mar, C. Fookes and P. K. D.V. Yarlagadda, “Automatic Solder Joint Defect Classification using the Log-Gabor Filter,” Advanced Materials Research Vols. 97-101, 2010.

Planned Publication

N. S. S. Mar, C. Fookes and P. K. D.V. Yarlagadda, “Design of Automatic Vision-based Inspection System for Solder Joint Classification”

N. S. S. Mar, C. Fookes and P. K. D.V. Yarlagadda, “Solder Joint Defect Classification using the Log-Gabor Filter, Discrete Cosine Transform and Discrete Wavelet Transform,”

Chapter 1

Introduction

Machine vision and image processing techniques provide innovative solutions in the direction of industrial automation [1]. The industrial activities have improved from the use of machine vision and image processing technologies on manufacturing processes. These activities include delicate electronics component manufacturing [2], quality textile production [3], Integrated Circuits (IC) manufacturing [4] and many others. [5]. In some industries, inspection tends to be tedious, difficult and dangerous where machine vision can be effectively applied. Machine vision technology increases productivity and provides a competitive advantage to industries by using this technology. This system is fast enough to meet the speed requirements of the application environment. A cost saving feature of industrial vision systems is the ability to meet the speed requirements of an application without the need of special purpose hardware and achieves the required production rate.

Conventionally, visual inspection and quality control are performed by human inspectors. Although human inspectors can do the job better than machine inspection in many cases, they cannot perform well due to the tiresome nature of manual inspection and the high rate of production. Recently, the development of automatic visual inspection systems has replaced human inspection on the assembly line. The application of machine vision for automated solder joint vision is more challenging than many other visual inspection problems. Since solder joint inspection requires accurate interpretation of shape information about the solder joint surface, better inspection systems are needed to fill the gap between available inspection capabilities and industry systems.

1.1 Motivation and Overview

The attachment of electronic components to Printed Circuit Boards (PCBs) has been accomplished generally by solder joining technologies over the past few decades. Inspection of solder joints has been a critical process in the electronics manufacturing industry to reduce manufacturing costs, improve yield, and ensure product quality and reliability. Traditionally, solder joint inspection has been performed manually or indirectly via electrical testing. Both methods are subject to human error and are inefficient. Monganti and Erical [6] compared manual and Automatic Optical Inspection (AOI) with the following criteria: 1) AOI relieves human inspections of the tedious jobs involved. 2) Manual inspection is slow and costly and does not assure high quality. 3) Production rates are so high that manual inspection is not feasible. 4) The industry has set quality levels so high that sampling inspection is not applicable. Besides, AOI has the following advantages that contact testing does not have. 1) AOI provides strict product control from the onset of production 2) AOI is a non-contact inspection, thus avoiding mechanical damage.

Recently, with the development of new Surface Mount Technology (SMT), the need for automatic inspection is ever increasing [7]. The current trends toward miniaturisation of components, surface mounting technology, and highly automated assembly equipment make the task of detecting the solder joint defects more critical and more difficult [8].

Currently available non-contact solder joint inspection technologies can be categorised into visual or optical inspection, X-ray inspection, thermal inspection and acoustic inspection. Several visual inspection systems for solder joints have been developed [8-11] with different illumination and classification techniques. Since many of these techniques and systems are suited for specific inspection tasks, the advance inspection techniques have a long way to go to meet industry requirements. New inspection techniques are urgently needed to fill in the gap between available inspection capabilities and industry requirements of low-cost, fast-speed, and highly reliable inspection systems.

1.2 Aim and Objective

Currently available solder joint inspection technologies are visual or optical inspection, X-ray inspection, thermal inspection and acoustic inspection. However, those inspection techniques are suited for specific inspection tasks and they do not necessarily encompass all the capabilities needed for evaluating the quality of the overall assembly [12]. The benefit and limitation of the above techniques are mentioned detail in Chapter 2. This research project aims to provide a solution for the automatic detection, localisation, segmentation and classification of solder joint defects on PCBs under different illumination conditions. The specific aims of this thesis are

(i) To investigate and evaluate the use of illumination normalisation on PCBs under different illumination conditions by using the Discrete Cosine Transform (DCT).

(ii) Investigate colour space for the effective detection of solder joints from the background.

(iii) Investigate the Gabor filter technique with the aim of extracting the feature vectors from solder joints.

(iv) Also examine the Discrete Wavelet Transform (DWT) and the DCT to extract the feature vector from solder joints.

(v) Determine and evaluate Mahalanobis Cosine distance measure to calculate the individual score from three classifiers.

(vi) Determine and evaluate methods for recombining output from correlated classifiers.

1.2.1 Outline of Thesis

The remainder of the thesis is organised as follows:

Chapter 2 provides background material related to the established field of classification of solder joint defects. A comparison of emerging algorithm for classification of solder joint defects is given. The resources, such as databases, by which performance of classification algorithm can be measured, are described.

Chapter 3 presents an automatic vision-based inspection system for solder joint segmentation. This is also referred to as the “front-end” inspection system of solder joint inspection. The front-end inspection system includes the detection, localisation and segmentation of solder joints. Experimental results on PCBs are presented to evaluate the performance of the system.

Chapter 4 examines methods for extracting the feature vectors from solder joint images and the algorithm for classification of defect solder joints. The classification correctness is evaluated by Detection Error Trade-off (DET) curves. Experimentation and analysis using these methods are also demonstrated.

Chapter 5 examines a method to perform score fusion from the Gabor filter, DWT and DCT. Further testing demonstrates the improved performance by combining multiple sources of information.

Chapter 6 summarises the research conclusions and proposes areas for future research.

1.3 Original Contribution of the Research in Knowledge Gap and Industry

In this research, an illumination normalisation approach is applied to an image, which can effectively and efficiently eliminate the effect of uneven illumination while keeping the properties of the processed image the same as in the corresponding image under normal lighting conditions. The proposed system does not need a special illumination system or a positioning system. The PCB images can be acquired by an ordinary camera. These normalised images are insensitive to illumination variations and are used for the subsequent solder joint detection stages. In the segmentation approach, each solder joint is correctly detected from the background image.

As was previously published in [13, 14] a method of achieving a robust classifier called Gabor filter is presented. Log-Gabor filters demonstrate the greater stability in the recognition of solder joint defects. Further testing demonstrates the performance advantage of the Log-Gabor filters, over both the DCT and DWT. A distance measure based on the Mahalanobis Cosine metric is also presented for classification of five different types of solder joints. Five different types of solder joints to be inspected included good solder joint, excess solder joint, insufficient solder joint, no solder joint and bridge solder joint. Linear classifier score fusion is demonstrated to achieve a high classification rate by combining the information from these classifiers.

The research presented in this dissertation proposes in the development of an automated non-contact, non-destructive and low cost solder joint quality inspection system. It is also expected to be applicable to many types of surface mount devices such as chip resistors and capacitors and conventional lead frame packages, making it a versatile and cost-effective automated manufacturing tool. This tool could be used on-line as a go/on-go inspection tool, and off-line during process development for process optimisation. Use of this solder joint defect inspection technology for automated manufacturing inspection will bring great cost savings by catching defects early in the process. This could lead to reducing the time to market new products, and allowing better process optimisation before manufacturing ramp-up.

Chapter 2

Review of Solder Joint Classification System

2.1 Introduction

Automatic Optical Inspection (AOI) plays a very important role in the automatic production process of Printed Circuit Boards (PCBs). Automatic industrial inspection systems for PCBs can be categorised into two important classes: contact methods and non-contact methods. Low inspection speed and high cost are disadvantages of contact methods. Additionally, they cannot detect non-electrical defects such as line width or spacing reductions. On the other hand, non-contact methods can improve the classification capabilities in terms of speed, low cost and highly reliable inspection systems. Advanced technology in computing hardware, image processing, pattern recognition and artificial intelligence have led to more effective and cheaper equipment for industrial visual inspection in the electronics manufacturing industry, especially in Surface Mounting Technology (SMT) [15].

In SMT, solder joints are significantly smaller, more abundant per unit area and more susceptible to soldering defects [16]. In SMT, components are mechanically redesigned to have small metal tabs or end caps that could be directly soldered to the surface of the PCBs. Components become much smaller and component placement on both sides of a board become far more common with surface mounting than through-hole mounting, allowing much higher circuit densities. Surface mounted devices are usually made physically small and lightweight for this reason. Surface mounting lends itself well to a high degree of

automation, reducing labour cost and greatly increasing production rates. Because the surface mount components are small and can be mounted on either side of the boards, they have achieved widespread usage.

The benefits of SMT are available in both design and manufacturing. Among the most important design-related benefits are significant savings in weight and electrical noise reduction. SMT also provides improved shock and vibration resistance as a result of the lower mass of components. In SMT, the solder joint serves as both the electrical and mechanical interface between component and substrate. However the amount of solder available is generally much less than at through-hole joint so its mechanical strength is less. Since leads do not penetrate the board, they cannot reinforce the joint. Proper joint formation is therefore critical to the reliable of the assembly. Post-solder inspection of solder joints defects and eliminates process defects and enables data acquisition for quality assurance and control.

The most commonly used inspection technologies are the in-circuit test, the functional test, the automated or manual inspection or other means. In-circuit test offers the distinct advantage of verifying the correct operation of a circuit. Unfortunately, as circuits continue to grow in complexity, the task of testing the circuit becomes more difficult. In addition, insufficient and missing solder joint which provide limited connection may not be detected with electrical testing and the circuit will fail after exposure to mechanical and thermal stresses.

However, PCBs manufacturers find those inspection methods too expensive and time consuming for a complex board. For this reason AOI is gradually replacing human inspection on the assembly line. AOI typically uses visible light and cameras to acquire the images of the PCBs. Classification algorithms are applied to verify different types of solder joint defects. In addition, the AOI system is capable of recording all the results and comparing them with all the other process parameters. Krippner [17] shows that 90% of the faults are components and soldering faults which are detectable only after soldering. Moreover, 80% of the optically recognisable faults could not be detected electrically. This result proves that optical inspection is necessary.

New inspection techniques for solder joints have been a critical process in the electronics manufacturing industry to decrease manufacturing cost, improve yield, and to ensure product quality and reliability [12]. Conventionally, solder joint

inspection has been performed manually and/or indirectly via electrical testing. Both methods are inefficient in term of human error.

Currently available solder joint inspection technologies fall into one of the four categories:

- Visual or optical inspection,
- X-ray inspection,
- Thermal inspection, and
- Acoustic inspection.

2.2 Survey of Solder Joint Non-Destructive Inspection Methods

This section surveys non-destructive methods for inspection that are applicable to solder joints. Both commercially available inspection systems and inspection methods still in research are reviewed.

2.2.1 Visual Inspection

Visual systems are the most commonly used non-destructive technique for the inspection of solder joints. Dedicated PCB inspection systems are available in 2D system, 3D system and holographic inspection. A basic 2D inspection system includes an illumination source to light up the object, a camera to record the image and image processor to produce a recognisable image. Subsequently, the image can be processed by using the digital image processing technique. Capson [9, 18] introduced tired illumination source which uses two circular colour lamps and one camera to highlight the joint's structure as shown in Figure 2.1 Images are acquired using a solid state colour TV camera and are digitised and stored using an RGB image capture board which samples the composite video signal from the camera into pixels [9]. The digitised colour images are processed by the personal computer. Colour highlight patterns are generated on the solder joint surfaces which are used for inspection of the solder joint.

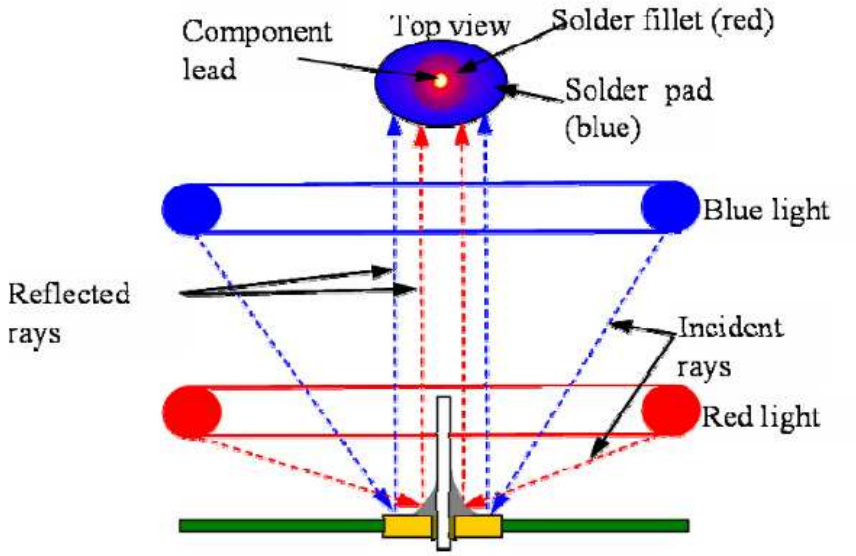

Figure 2.1 : Schematic of tired-colour illumination solder joint inspection system with two circular colour light [12]

As shown in Figure 2.2, a three colour tiered illumination system is implemented [19]. The lamps are coaxially tiered in a sequence of green, red and blue moving upwards from an inspection surface. Although, three different light colours are turned on simultaneously, the same effect is obtained when each lamp is turned on one at a time. This can reduce the time involved in scanning a large number of point sources.

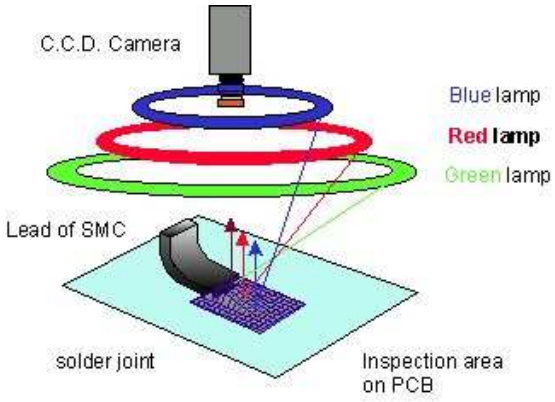

Figure 2.2 : Schematic of tired-colour illumination solder joint inspection system with three coloured lights [19]

Another important method for determining the solder joint inspection is known as laser triangulation which can provide faster data acquisition [20-22]. A

laser beam is projected to the sample's surface being measured. The reflected light is collected by a light sensitive digital detector array know as photodetectors [22]. Figure 2.3 shows a typical configuration of laser triangulation. The reflected light is varied according to the height of the sample surface as the beam scans across the sample's surface. Many commercial Automated Optical Inspection (AOI) systems have incorporated laser triangulation for various purposes of visual inspection system.

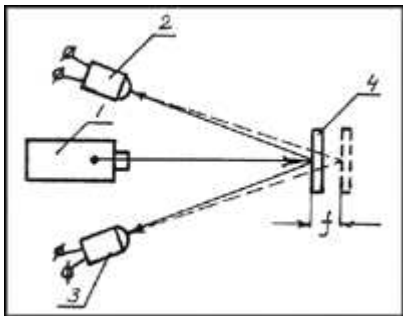

Figure 2.3 : Laser triangulation measuring system , f = displacement, 1 = laser light source, 2 and 3 = light sensors, 4 = surface [12]

Nakagawa [23] has developed a structured light method which included projecting a narrow beam of light onto the joint at various positions and then using the spectrometry to get information of the solder joint based on the geometric relation.

2.2.2 X-Ray Inspection

X-ray solder joint inspection is a promising alternative for solder joint inspection [12]. A common system has an X-ray source to generate radiation, an X-ray conversion screen to collect the penetrated radiation and a video camera to convert the photons on the screen to digital form. This system is efficient and detects most of the solder joint defects.

2.2.3 Thermal Inspection

Thermal inspection can be used to measure if the solder joints have a specific heat capacity [12]. In this inspection system, the whole PCB assembly is exposed to an

Infrared heat source. The released thermal energy is varied depending upon the different type of solder joints.

2.2.4 Acoustic Inspection

In acoustic inspection, sound waves are essentially mechanical vibrations of the medium in which they travel. Solder joints can be inspected by the joint's resonant frequency generated by sound wave vibration [12].

Among these techniques, some are well established and have been commercially available for practical use while others are still on-going trying to meet the industry requirements of low-cost, fast-speed, and highly reliable inspection systems.

2.3 Illumination Design

The imaging of solder joints is a difficult task in automated visual inspection technology due to the specularity of the solder joint surface. Reflections of the specular solder joint may appear or disappear even with small changes in viewing direction [24]. Moreover, specular surface hardly has a smooth shading that matches its shape which makes it complex to recognise a specular surface from visual information. The different shape of solder joint is also a challenge to develop an automatic solder joint inspection system. The shape of the solder joints tends to vary with soldering conditions. Even those classified into same type of solder joints are slightly different in shape when carefully examined. To overcome this problem, several researchers have tackled it by using proper illumination system which can maintain sufficient illumination levels to reveal the darker regions of the solder joint image.

Bartlet et al [8] used four overhead fluorescent lamps and one fluorescent ring lamp to effectively inspect solder joints and avoid shadows in the captured image. Capson [9] used a tiered-colour illumination method to generate colour contours onto the solder joints. This illumination system consisted of red and blue circular fluorescent lamps with different heights. By examining the contour shape measured by geometric descriptor, solder joint defects could be determined. The lighting arrangement allows direct correlation between solder joint profile and

colour planes. The colours of the lights also aid in segmentation of the solder joints from the PCB.

Kim, Ko and Cho [7, 24] improved the previous system by using three colour circular lamps (Red, Green, Blue) with different illumination angles. Three different types of image are sequentially captured as three layers of lights are turned on one after another and obtained 2D and 3D features of the images. An attractive approach for an illumination system is developed by using only one layer of tiered light and two features [25]. Insufficient, acceptable and excess solder joints are classified by two straight lines on the 2D feature plane. The number of circular illuminations can be reduced to one when the incident angle is optimised. Among the 62 images, three are mis-classified resulting in a recognition rate of slightly better than 95%. This method significantly saves time for image scanning and computation compared to previous illumination systems. However, the processing of colour images required very high over-heads in terms of computation and complex processing.

Meanwhile, a hemispherical lighting system with a structured LED array was developed with a CCD camera to take gray-level images sequentially [26]. The structured LED array is placed on the lighting system to project light from different positions onto the solder joint surface. A slant map was used to extract information from the images based on the slant angles which represent the solder joint shape and are directly relative to the quality of the solder joint. This system achieves 7.69% of overall fault alarm ratio.

Ong [27] combined orthogonal and oblique gray-level images with the use of two viewing direction configurations, namely, the orthogonal view and oblique view. For orthogonal images, a camera was set up perpendicular to the plan of the PCB. A viewing direction inclined approximately 40 degree to the vertical plan was used for oblique images. However, it is important to maintain high accuracy of the relative geometrical position of the cameras for a multiple camera setup.

Ahmed [15] used a simple method to capture images by using one CCD camera. The acquisition system was covered by a black screen and the PCB was illuminated by fluorescent lamps. This setting helps to control the illumination condition by avoiding external light source.

2.4 Classifier Design

In order to complete the inspection system, classifiers have been developed using different approaches to select features extracted from an image.

2.4.1 Statistical Pattern Recognition Approach

A pattern recognition system classifies solder joints based upon statistics obtained from a "training set" of each solder joint's class. The Bayesian and maximum likelihood classifier are a traditional statistical approach for classification. In this approach it is necessary to have the knowledge on probability distribution of each class and this requires a large number of experiments. Bartlet et al. [8] used minimum classifier to classify each solder joint into one of the two good types and seven defected types depending on five different features: basic gray level statistics, 3D gray level inertia features, faceted gray level surface area features, differential geometric gray level surface curvature features and binary image connected region features.

2.4.2 Rule Based Classification Approach

Rule based classification systems have been widely used in machine learning applications because of their easy to understand ability and interpretability. In some cases, this method needs counter measures against the appearance of unexpected members of a class. Capson [9] proposed a tree classifier by using geometric descriptors which measure the shape of the contours and the colour level intensities of the solder joint images. For board 'A', 93.5% of solder joint was correctly identified and for board 'B', a 76% success rate was achieved. The false alarm rates were 3.0 and 4.3 respectively. Another rule based classification system was also employed by using fuzzy set theory [28, 29]. This can be especially useful when objects are not clearly members of one class or another. In addition, fuzzy techniques will specify to what degree the object belongs to each class, which is useful information in solder joint recognition.

2.4.3 Artificial Neural Network Approach

In recent years, Artificial Neural Network (ANN) approach has been applied to Automatic Optical Inspection (AOI) systems due to learning capability and nonlinear classification performance. ANN can be divided into the unsupervised ANN and the supervised ANN. Multilayer neural network is one of the supervised neural networks and has been applied to solder joint application [24]. Kim proposed the neural network with two following modules: a processing module and trainable module. The first module is designed to implement the calculation of the correlations in functional terms and the second module is design to learn about solder joint classification as a human inspector. The advantage of a multilayered neural network is the ability of learning human experiences. However, the complexity of solder joint shapes causes the neural network's convergence rate to become poor.

The other neural network approach is an unsupervised neural network such as a Learning Vector Quantization (LVQ) neural network [19]. LVQ method is good for pattern classification because of their fast learning nature, reliability and convenience of use. One disadvantage for LVQ is that it cannot sometimes produce a correct decision for complex classification problems. Kim [19] applied an adaptive learning mechanism to correct the LVQ classifier. The adaptive learning mechanism can select the optimal number of prototypes set to achieve performance within an acceptable error rate. Again, Ong [27] proposed a new approach using a dual viewing angle imaging method with an ANN and learning vector quantization architecture. From the experimental results, this system has an improved recognition rate and resistance to noise. However, high accuracy on the relative geometrical position of the camera is required.

In order to improve the human knowledge in the classification of complex solder joint criteria, Ko et al. [30] combine a fuzzy logic scheme into the LVQ neural network. In the neural network module, three LVQ classifiers are used to cluster solder joints by using similarity between an input pattern and prototype patterns. In the fuzzy module, new classification criteria are generated using a pre-defined rule built by the inspectors. More accurate classification results can be achieved because expert knowledge is applied into the classification criteria.

Accianni [31, 32] extracted two feature vectors, the “geometric” feature vector and the “wavelet” feature vector, from the images and used a multiple neural network system to characterise solder joint defects on Printed Circuit Boards assembled in Surface Mounting Technology. Two feature vectors feed the multiple neural network system constituted by two Multi Layer Perceptron neural networks and the LVQ network for the classification. From the experimental result, the multiple neural network system achieved the best compromise in terms of recognition rate and time in respect to single MLP and LVQ network.

Other technique include ANN ensembles based machine vision inspection system which has also been developed [33]. This system uses a Genetic Algorithm to train many one layered perceptrons respectively as classifiers and combined linearly into an ensemble. To correct the trained ANN’s errors, the weights of training samples were adjusted by AdaBoost algorithm.

2.4.4 Other Classifier Designs

Meanwhile, many works and various techniques have been developed to classify the solder joint defects. Kim [7] developed a two stage classifier to recognise four types of solder joints: good, insufficient, excess and no solder joints. In the first stage, Multi Layer Perceptrons are used to roughly classify the image by the evaluation of 2D simple features. For some uncertain results, 3D features are classified based on the Bayes classifier.

Support Vector Machine (SVM) based method was also developed to inspect the solder joint quality [34, 35]. SVM produced a good classification result even with a small size of training data due to its ability to maximise the distance of each class. Jiang et al. [36] introduced a simpler method to identify the position of the solder joint and a tree structure classifier to categorise the solder joint defects. This methodology does not require special lighting or special equipment to capture the PCBs image. Pareto chart is also used to observe the average distance of different types of solder joints with respect to the various features i.e. binary image-based features and gray value-based feature.

Although many methods have been developed in this area, these methods need a complex system of image acquisition. It is important to select the right classification method to improve the detection rate under different lighting

conditions. This stage is not easy because each classification method presents advantages and disadvantages.

2.5 Knowledge Gap

In commercial PCB assembly processes, the solder joint inspection has one essential problem for quality control in the PCB assembly process. For accurate visual inspection, it is necessary to obtain the system that is not sensitive to variation of light and requires robust algorithm for classification. Since the solder joint surfaces are curved, tiny and specular reflective, it is difficult to determine the shape of solder joints from visual information. From the points of classification problem, although a set of solder joints belong to the same acceptable class of quality, the shapes are not identical to each other, but vary to a certain degree. For this reason, variations in the solder joint shapes have made it difficult to develop an automatic solder joint inspection system. Moreover, classification criteria for solder joints are usually based on human experience and can be changed according to the products. To overcome the limitation, complex systems of image acquisition that need special illumination system and several kinds of inspection algorithms are developed.

2.5.1 Knowledge Gap Identified

Many researches developed complex systems of image acquisition that need special illumination systems. In practice it is too time-consuming and costs to conduct comprehensive studies on illumination and specular reflection of solder joint. In order to use a simple hardware setup and no special lighting, one of the solutions is to conduct research on the proper illumination normalisation algorithm.

In addition, most of the methods described above used neural networks for images processing. The advantage of the classifier using a neural network is the ability of learning human experiences, but the disadvantage is when the input data space is too complex to determine decision boundaries for classification. The performance of the classifier may get worse due to the inability of the neural network to process complex input variables. Statistical approaches such as Bayesian and maximum likelihood classifiers require knowledge on the probability distribution of data that needs a large number of experiments to be done. A rule

based method has an advantage in using human skill to make classifications. But for the appearance of unexpected members that are not included in the construction rule, this method requires several measurements. Due to these reasons, the existing methods do not give good results when the inconsistency for solder joint shapes is encountered. In summary, most of the research which has been done on solder joint inspection demands a robust method for the classification algorithm.

2.5.2 Relationship between Indentified Knowledge Gap and Proposed Research

In this research, a new approach using illumination normalisation and Gabor filter technique is proposed to find out the solution for an automatic detection, localisation, segmentation and classification of solder joint defects. An illumination normalisation stage involves effective and efficient methods to eliminate the effect of uneven illumination while keeping the properties of the processed image the same as in the corresponding image under normal lighting conditions. Consequently special lighting and instrumental setup can be reduced in order to detect solder joints. These normalised images are insensitive to illumination variations and are used for the subsequent solder joint detection stages. In the segmentation approach, the PCB image is transformed from an RGB colour space to a YIQ colour space for the effective detection of solder joints from the background. From the experimental results, the proposed approach improves the performance significantly for images under varying illumination conditions.

A new technique for solder joint defect classification using the Gabor filter has been demonstrated to achieve high recognition rates and it is resistant to misalignment. This filter has also found favour in many image processing fields due to its desirable characteristic of spatial locality and orientation selectivity. Discrete Wavelet Transform (DWT) is also applied to extract feature vector from solder joint image. The advantage of DWT is that it can be treated as image-to-image transformation. This will enable each wavelet coefficient to be treated as a pixel image and thus allows the image difference operation to be carried out. In addition, Discrete Cosine Transform (DCT) has energy compaction property and good performance in illumination normalisation so DCT is also applied for feature extraction of solder joints. The feature scores are calculated by Mahalanobis Cosine

Distance and the results are evaluated by Detection Error Trade-off (DET) plot. The method for combining the information from these classification systems is also examined. Fused classification aims to improve the accuracy and robustness of a classification system. These information sources need to be complementary as redundant information will not improve verification. Classifier fusion combines the information from multiple verification systems that are achieved from three different classifiers. Classification improvement occurs for the classifier fusion by using linear classifier fusion. The methodology presented in this research can be an effective method to improve classification in solder joint defects.

A more detailed literature review and methodology related to the use of the Log-Gabor filter, DCT and DWT will be presented in Chapter 4 along with experimental results.

Chapter 3

Segmentation of Solder Joints

3.1 Introduction

All automatic inspection systems consist of an acquisition system and a pre-processing system to perform the classification of solder joint. The pre-processing stage is always included to extract Region Of Interest (ROI) from the acquired image in order to reduce an imperfect functioning of the system. Moreover, the specularity of the solder joint surface causes difficulties in the extraction of relevant information. Specular reflections of the solder joint surface may appear or disappear with small changes in viewing direction. Furthermore, the shape of the solder joints tend to vary greatly with soldering conditions including the amount of solder paste and heating level applied during the soldering process. Many of the researches reported in the literature require special lighting sources or set up because of the variety of solder joint shapes. Further research is required to address the development of robust and automated inspection systems which can operate in less constrained lighting environments to reduce the cost and utility of this technology.

The purpose of this chapter is to propose a pre-processing system, including localisation, illumination normalisation. The latter can be applied to an image effectively and efficiently to eliminate the effect of uneven illumination while keeping the properties of the processed image the same as in the corresponding image under normal lighting conditions and segmentation. An illumination variation under different lighting conditions can be significantly reduced by discarding low-frequency DCT coefficients. This approach does not require modelling step and

bootstrap sets. It is very fast and it can be easily implemented in a real-time recognition system.

The inspection procedure adopted and the image databases used in this research are presented before describing the methodology and experiments for the segmentation of solder joint images.

3.2 Inspection Procedure

The inspection procedure is summarised in the chart of Figure 3.1. There are four main tasks in solder joint classification: capture image, segmentation, feature extraction and classification. Several inspection algorithms and researches have been applied for each task. Figure 3.2 represents detailed methodology for solder joint defect classification followed by this research. The first step is acquisition of image. The image acquired by the camera contains the Region of Interest (ROI) and also useless zones for the diagnosis so that ROI is needed to extract from an acquired image. To extract ROI, the Hough Transform is utilised for automatic alignment of the PCBs. Afterwards the illumination normalisation technique is applied to an image which effectively eliminates the effects of uneven lighting conditions. After that the image is transformed from an *RGB* to a *YIQ* colour model for the effective detection of solder joints from the background. Then it is followed by thresholding, region filling and segmentation of solder joints. Each of these steps is described in Chapter 3 and has been published [37].

The next step of the diagnosis process is the feature extraction. In this step, features are extracted by three different methods; Log Gabor filter, DCT and DWT. Finally, these features are measured by Mahalanobis Cosine distance and five types of solder joint have been classified. Method for combining information is examined to improve the accuracy and robustness of classification of solder joint. The details of classification algorithm and classifier fusion are presented in Chapter 4 and Chapter 5 respectively.

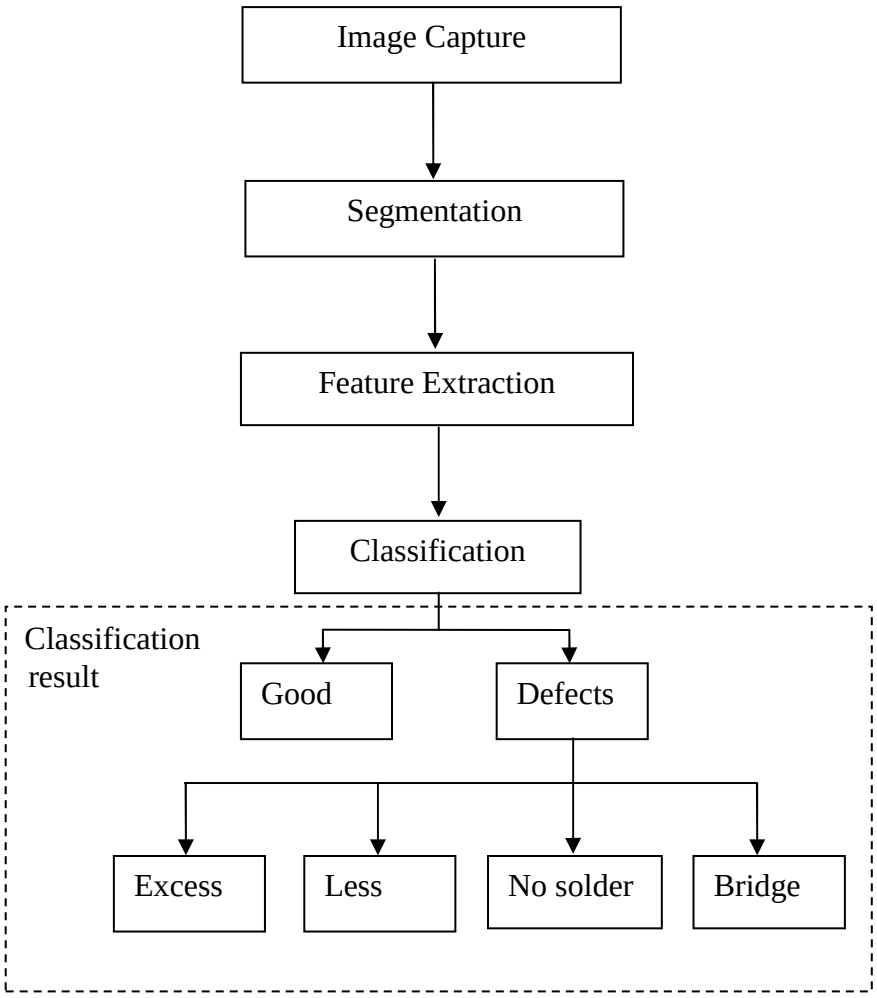

Figure 3.1: Basic inspection procedure for solder joint defect classification

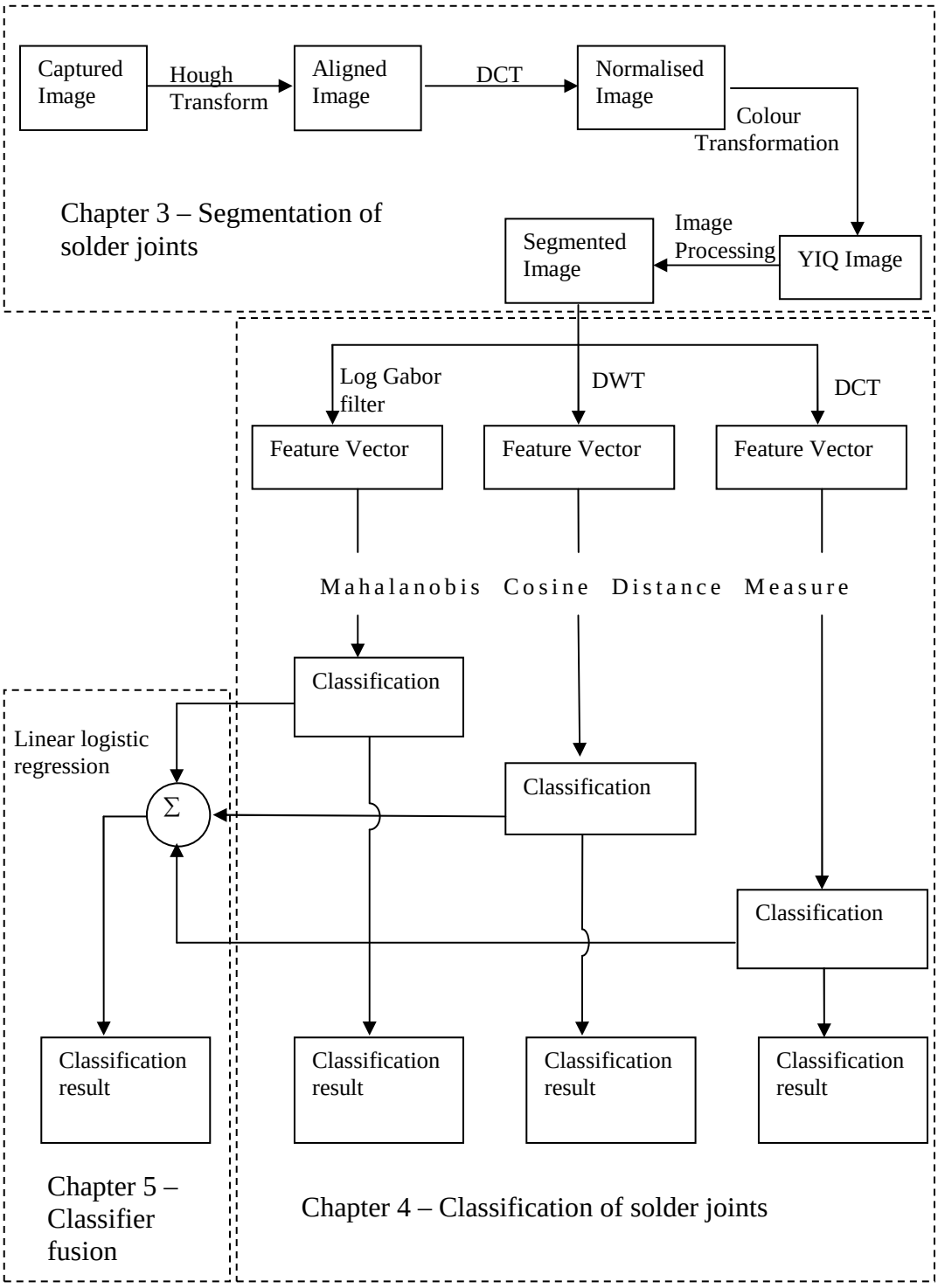

Figure 3.2 : Detail inspection procedure for solder joint defect classification

3.3 Databases

A number of datasets have been used to evaluate the methodologies and hypotheses laid out in this thesis. They are Database 1, Database 2 and Database 3.

Each of the databases has a different number of subjects and acquisitions, in addition there are imaging conditions which are particular to each database. Database 1 is supported from Ahmed Nabil Belbachir (Vienna University of Technology). In this image acquisition system, an XY positioning system controls all the displacements of the CCD camera [15]. The dimension of the framed region is controlled by modifying the lens zooming. In order to control the illumination conditions, the acquisition system is covered with black screens that avoid external light sources. The circuit under test is illuminated using commercial fluorescence lamps. Database 1 is used for automatic segmentation of solder joint.

Database 2 is supported by MRD Rail Technologies and the PCB images are captured by normal digital camera under a fluorescent light source in the lab. There are no special illumination systems or advanced X-Y positioning systems. Database 2 is especially used for segmentation. Since the height of the camera from the image is inconsistent when acquiring the image, it is not suitable to use in classification.

Due to the above mentioned problem, the acquisition system for image Database 3 is fixed at a certain height. The acquiring system for image database 3 is constituted by a digital camera mounted on a fixed position and acquires the image of the PCB under test. This acquisition system does not use special illumination system and advance X-Y position system. Sample image for three databases are shown in Figure 3.3, Figure 3.4 and Figure 3.5.

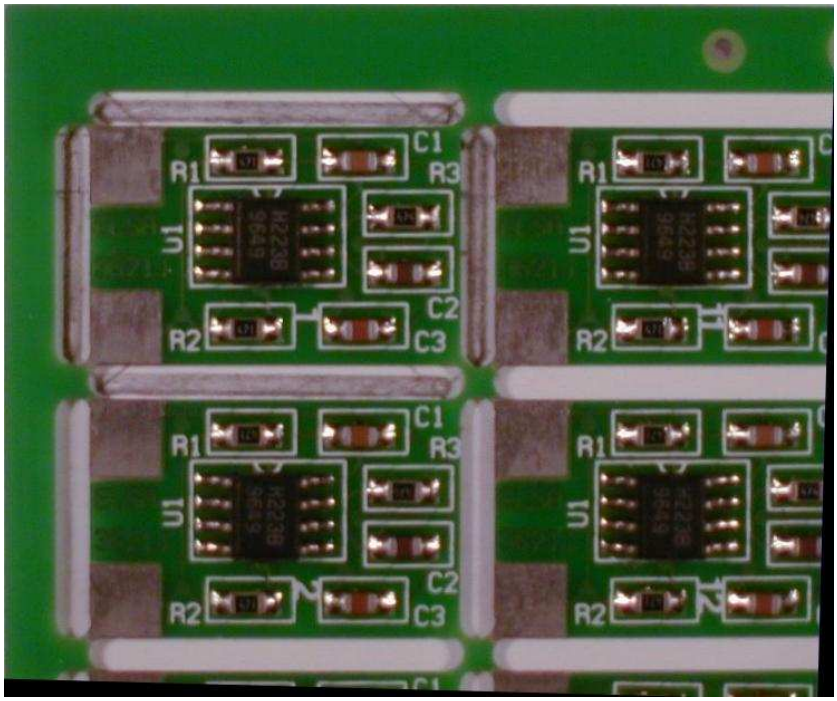

Figure 3.3 : Sample image for database 1

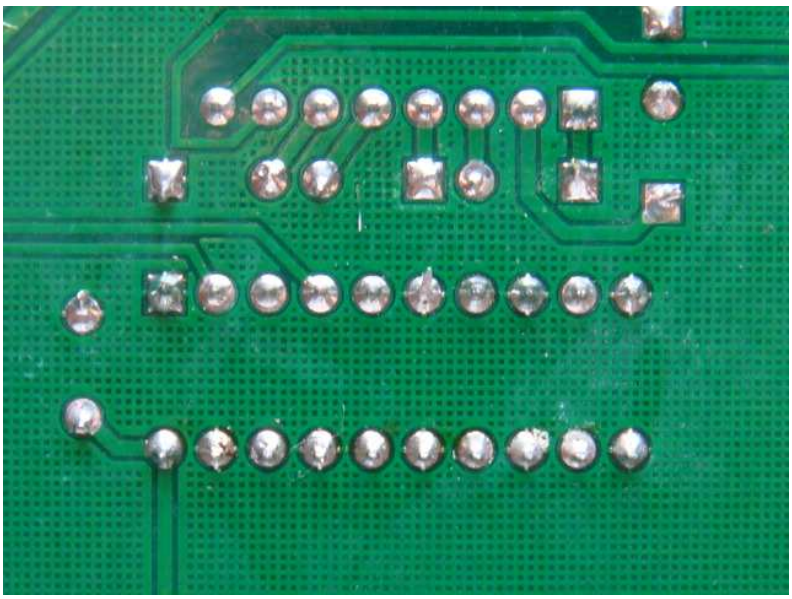

Figure 3.4 : Sample image for database 2

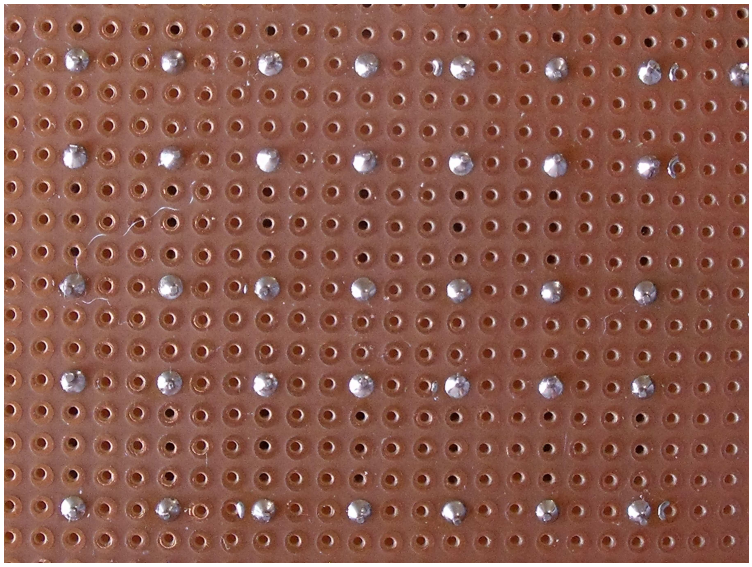

Figure 3.5 : Sample image for database 3

3.4 Hough Transform

The Hough transform is a powerful method for detecting edges. It transforms between the Cartesian space and a parameter space in which a straight line can be defined. The advantage of the Hough transform is that the pixels lying on one line need not all be contiguous. This method is very useful when trying to detect lines with short breaks in them due to noise, or when objects are partially occluded. For this reason, the Hough transform technique is used to locate the PCB so that the PCB does not need to be placed onto a precision X-Y table. In this way the PCB can be located on an automatic conveyor line, without interrupting the line production. This algorithm also helps to improve accuracy of the solder joint segmentation.

The Hough Transform method has been recognised as one of the most popular methods to extract parameterised lines from an image. The proposed Hough Transform function is implemented in Matlab 7.4.0287 (R2007a) [38]. The transform maps a line in the image space (x,y) into a point in the Hough Transform parameter space. For straight line detection, the equation of a line can be expressed as:

$$\rho = x \cos(\theta) + y \sin(\theta), \quad (3.1)$$

where θ and ρ are respectively the orientation of the line and the distance to the origin.

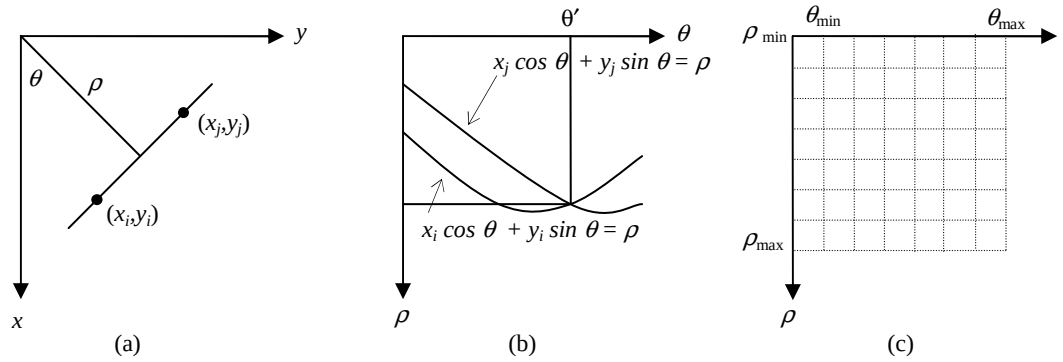

Figure 3.6 : (a) (ρ, θ) parameterization of lines in the xy-plane. (b) Sinusoidal curves in the $\rho\theta$ - plane; the point of intersection, (ρ',θ'), corresponds to the parameters of the line joining (x_i, y_i) and (x_j, y_j). (c) Division of the $\rho\theta$ - plane into accumulator cells [39].

Figure 3.6 (a) illustrate the geometric interpretation the parameters ρ and θ [39]. A horizontal line has $\theta = 0^\circ$ with ρ being equal to the positive x-intercept. Similarly, a vertical line has $\theta = 90^\circ$, with ρ being equal to the positive y-intercept, or $\theta = -90^\circ$, with ρ being equal to the negative y-intercept. Each sinusoidal curve in Figure 3.6(b) represents the family of lines that pass through a particular point (x_i, y_i). The intersection point (ρ',θ') corresponds to the line that passes through both (x_i, y_i) and (x_j, y_j). The Hough transform arises from sub-dividing the $\theta\rho$ parameter space into accumulator cells, as illustrated in Figure 3.6 (c), where (ρ_{min}, ρ_{max}) and (θ_{min}, θ_{max}) are the expected ranges of the parameter values. Usually, the maximum range of values is $-90^\circ \leq \theta \leq 90^\circ$ and $-D \leq \rho \leq D$, where D is the distance between corners in the image. The cell at coordinates (i, j) with a accumulator value A(i, j), corresponds to the square associated with parameter space coordinates (ρ_i, θ_i). Initially, these cells are set to zero. Then, for every non-background point (x_k, y_k) in the image plan, let θ is equal each of the allowed subdivision values on the θ axis and solve for the corresponding ρ using the equation $\rho = x_k \cos\theta + y_k \sin\theta$ The resulting ρ-values are then rounded off to the nearest allowed cell value along the ρ-axis. The corresponding accumulator cell is then incremented. At the end of this procedure, a value of Q in $A(i, j)$, means that Q points in the xy-plane lie on the line x

cos θ_j + y sin θ_j = ρ_i. The number of subdivisions in the $\rho\theta$- plane determines the accuracy of the colinearity of these points.

In Figure 3.7 and Figure 3.8 show the image before and after applying the Hough transform technique. The figures clearly show how the image has been rotated to ensure that the PCB is correctly oriented in the horizontal and vertical directions.

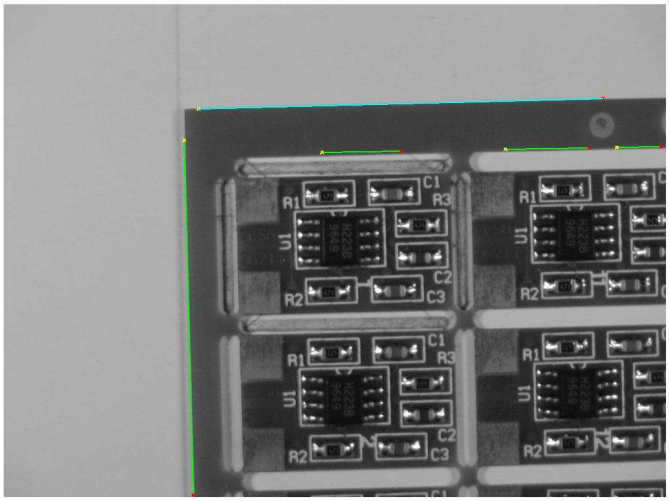

Figure 3.7 : Acquired image

Figure 3.8 : Result of Hough Transform

3.5 Normalisation Illumination

Since reflections of the specular solder joint surface may appear, disappear, or change their patterns unexpectedly, even with small changes in lighting condition, it results in a challenge for this research. The same solder joint can appear greatly different under varying lighting conditions. There is a need to normalised an image under different lighting. In this approach, images are normalised using Discrete Cosine Transform (DCT) techniques to appear stable under different lighting conditions. A useful aspect of DCT is the ability to physically interpret the basis functions. The position of coefficient reflects the corresponding sum of pixel value in the block. The 0^{th} coefficient represents the lowest frequency band in DCT. Since illumination variations mainly lie in the low-frequency band, an appropriate number of DCT coefficients are truncated to minimise variations under different lighting conditions [40] . There are four established types of Discrete Cosine Transforms (DCT's), i.e., DCT-I, DCT-II, DCT-III and DCT-IV. The DCT-II is more widely applied in signal coding. The 2D *M* x *N* DCT is defined as [40]:

$$D(u,\upsilon)=\alpha(u)\alpha(\upsilon)\sum_{x=0}^{M-1}\sum_{y=0}^{N-1} f(x,y)\times\cos\left[\frac{\pi(2x+1)u}{2M}\right]\cos\left[\frac{\pi(2y+1)\upsilon}{2N}\right], \quad 3.2$$

and the inverse transform is defined as

$$f(x,y)=\sum_{u=0}^{M-1}\sum_{\upsilon=0}^{N-1}\alpha(u)\alpha(\upsilon)D(u,\upsilon)\times\cos\left[\frac{\pi(2x+1)u}{2M}\right]\cos\left[\frac{\pi(2y+1)\upsilon}{2N}\right], \quad 3.3$$

where

$$\alpha(u)=\begin{cases}\frac{1}{\sqrt{M}}, u=0\\ \sqrt{\frac{2}{M}}, u=1,2,...,M-1\end{cases}.$$

$$\alpha(\upsilon)=\begin{cases}\frac{1}{\sqrt{N}}, \upsilon=0\\ \sqrt{\frac{2}{N}}, \upsilon=1,2,...,N-1\end{cases}$$

In the proposed approach, the DCT is performed on the entire image to obtain all frequency components of the image. The proposed DCT function is implemented in Matlab 7.4.0287 (R2007a) [38]. This block matrix consists of DCT coefficients, D_{uv}. The top-left coefficient, c_{00} is correlated to the low frequencies of

the original image block. As c_{00} is removed, the DCT coefficients correlate to higher and higher frequencies of the image block, where c_{uv} corresponds to the highest frequency. It is important to eliminate the low frequency which is the most sensitive to human eye. The manner of discarding DCT coefficients is shown in Figure 3.9.

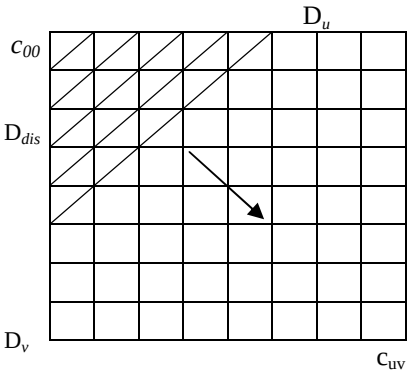

Figure 3.9 : Manner of discarding DCT coefficients (only the first 8 x 8 coefficients are shown)

Figure 3.10 : Original image

Figure 3.11 : Reconstructed image by applying the DCT

As illustrated in Figure 3.10 and Figure 3.11, the original image is improved by applying the DCT.

3.6 Colour Transformation

It is not easy to separate the solder joints and other background from a PCB image, because there are many lines and markings that have similar values as the solder joint [36]. In this case, the PCB image is transformed from *RGB* colour model to *YIQ* colour model. The advantages of *YIQ* colour model are 1) processing *Y* component only will differ from unprocessed image in its appearance of brightness and 2) most high frequency components of a colour image are in *Y*. The image is transformed to *YIQ*, which gives one luminance signal *Y* and two colour signals *I*&*Q*. Again, I stands for in-phase, while *Q* stands for quadrature, referring to the components used in quadrature amplitude modulation [41]. Equation 3.4 and 3.5 describe the transformations between the *RGB* and *YIQ* colour spaces,

$$\begin{bmatrix} Y \\ I \\ Q \end{bmatrix} = \begin{bmatrix} 0.2290 & 0.5870 & 0.1140 \\ 0.5957 & -0.2744 & -0.3213 \\ 0.2115 & -0.5226 & 0.3111 \end{bmatrix} \begin{bmatrix} R \\ G \\ B \end{bmatrix} \text{ and} \qquad 3.4$$

$$\begin{bmatrix} R \\ G \\ B \end{bmatrix} = \begin{bmatrix} 1 & 0.9563 & 0.6210 \\ 1 & -0.2721 & -0.6740 \\ 1 & -1.1070 & 1.7046 \end{bmatrix} \begin{bmatrix} Y \\ I \\ Q \end{bmatrix} \qquad 3.5$$

3.7 Localisation of Solder Joint

3.7.1 Thresholding

After performing the colour transformation of an image, a solder joint needs to be extracted from its background by a threshold selection. If the object has a different average gray level from that of its background, it is often difficult to select an appropriate threshold. In this research, a successive iterative process is described to get an optimum threshold [42]. The histogram of an image is initially segmented into two parts using a starting threshold value such as half the maximum dynamic range. Then, the sample data are computed into two classes which are the sample mean of the gray values associated with the foreground pixels and the sample mean of the gray values associated with the background pixels. Then a new threshold value is computed as the average of the above two sample means. The resultant threshold and its upper and lower thresholds are applied to the PCB image. Then the new threshold value is calculated according to the number of components detected. This process is repeated until the numbers of components do not change any more. This procedure is implemented in Matlab 7.4.0287(R2007a) [38].

3.7.2 Region Filling

Although the solder joints have been detected, closed or opened holes might occur on solder joints after segmentation because of the surface property and shape of solder joints [43]. The soldering conditions, the amount of solder paste cream and the heating level during the soldering process define the surface property and shape of solder joints. These holes can be confusing when determining the solder joint location. So those holes need to be mended. Firstly, erosion and dilation of Morphology is applied to enclose an opened hole. If dilation of Morphology is used to enclose a hole, it might change the original shape of the solder joints. In that case, Region Filling is applied to mend these closed holes. Region Filling is based on set dilations, complementation, and intersections [44]. In Figure 3.12, *A* denotes a set containing a subset whose elements are 8-connected boundary points of a region.

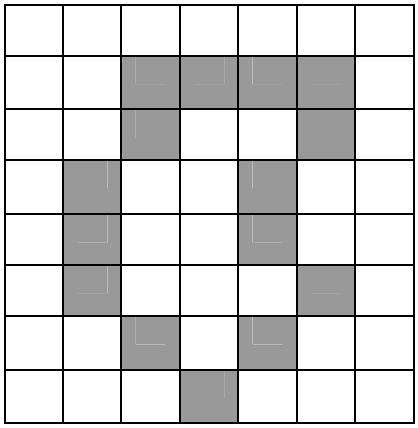

Figure 3.12 : Set A

Beginning with a point *p* inside the boundary, the objective is to fill the entire region with 1's. All background points are labelled 0, and 1 is assigned to *p* at the first time of iteration. The following equation is used to fill the region with 1's:

$$X_k = (X_{k-1} \oplus B) \cap A^c \qquad \text{k= 1, 2, 3, …} \qquad 3.6$$

where $X_0 = p$, and B is the symmetric structuring element. The algorithm terminates at iteration step k if $X_k = X_{k-1}$. The set union of X_k and A contains the filled set and its boundary.

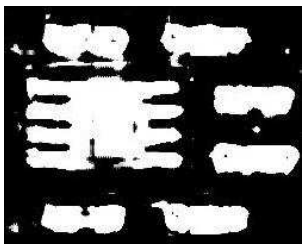

(a)

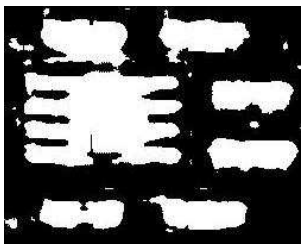

(b)

Figure 3.13 : (a) Solder joint image before the region filling (b) Solder joint image after the region filling

Figure 3.13 (a) shows an image composed of white joints with black inner spots. An image such as this might result from thresholding into two levels. The dark spots inside the spheres are the result of reflections. These dark spots are eliminated by using region filling so that the components can be extracted from the background more accurately. Figure 3.13 shows before and after the region filling is applied.

3.7.3 Segmentation Process

There are two stages in the segmentation process. In the first stage of segmentation, components are extracted from the acquired image and the next step is to extract an image of the solder joint from each component. The detected components can be IC chips, resistors, capacitors and so on.

In performing the first step of segmentation, the pixels which represent component and background are grouped into meaningful regions [45]. The white pixels correspond to component and the black pixels correspond to background. Once an object pixel is found, the entire connected object region is enumerated. Finally, the centroid of the region is calculated as a simple measure of object location. Figure 3.14 shows the image after applying the segmentation on the PCB board by defined the boundary around the components.

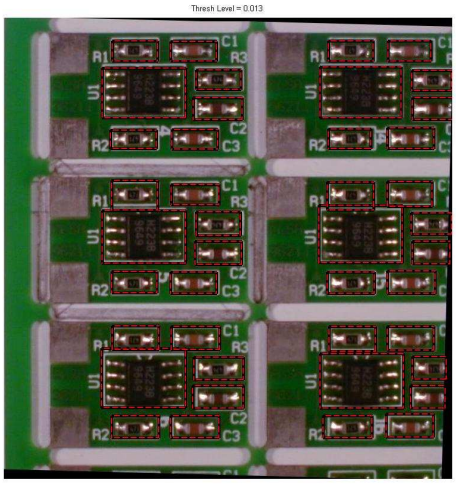

Figure 3.14 : An example of detected components from database 1

For the next step of segmentation, each solder joint can be isolated by projection of the image horizontally and vertically. Each lead-pad pair can be isolated by vertical projection and the solder region can be identified by horizontal projection (Figure 3.15). Suppose p x m is a matrix associated with the thresholded image. The equations for the horizontal projection H and the vertical projection V are defined as follows:

$$H = \sum_{i=1}^{p} \lambda_i \text{ and} \qquad 3.7$$

$$V = \sum_{j=1}^{m} \gamma_j \,, \qquad 3.8$$

where λ_i and γ_j are the i-th row and j-th column of the image. In this stage, the images of each solder joint can be extracted from the component. Figure 3.16 and Figure 3.17 show the result of detected solder joints which are marked with red box.

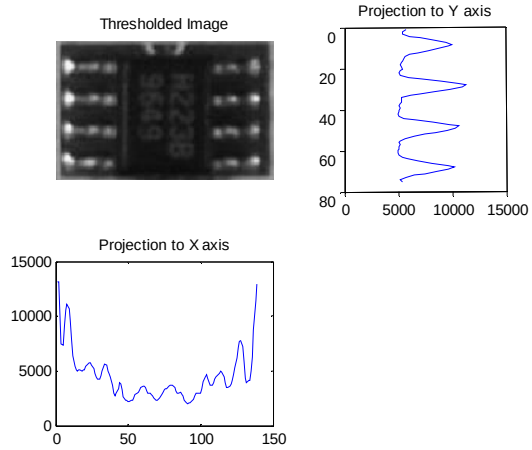

Figure 3.15: Image processing of solder joint

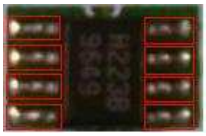

Figure 3.16: An example of detected solder joints from database 1

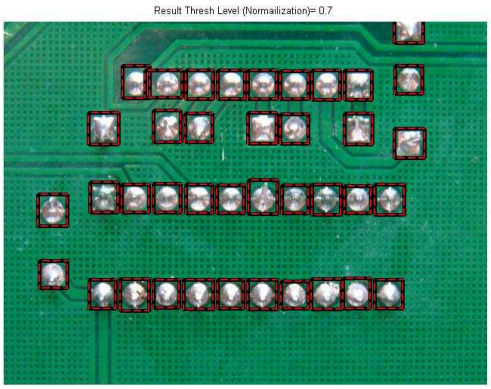

Figure 3.17: An example of detected solder joints from database 2.

3.8 Experimentation and Result

Two sets of solder joint databases, (1) and (2), were used in the analysis. The total of 3840 (database 1) and 621 (database 2) solder joints were used in these experiments. The parameter such as the size of solder joints is approximately defined. Three indices were used to evaluate the segmentation results:

Hit rate: percentage of correctly detected joints

Miss rate: percentage of undetected joints

False rate: percentage of incorrectly detected joints

Four different types of experiments were performed on solder joint images to identify the best segmentation algorithm. The first experiment was conducted with the combination of two algorithms; normalisation illumination and automatic thresholding which gives the best result with a 99.93% success rate. The second experiment is performed for automatic thresholding without illumination normalisation. The third and fourth experiments were performed for manual thresholding with and without illumination normalisation. The manual threshold value is selected by plotting the resultant thresholding value from automatic thresholding and selecting its mean value. From these experiments, it can be clearly seen that the success rate is very low for manual thresholding without illumination normalisation with a 78.94% success rate. The results of the test stage are summarised in Table 3-1 and Table 3-2 for database 1 and 2.

Condition of experiment	Hit rate (%)	Miss rate (%)	False rate (%)
(1). Automatic thresholding with illumination normalisation	99.93	0.07	0
(2) Automatic thresholding without illumination normalisation	99.70	0.3	0
(3) Manual thresholding with illumination normalisation	97.56	2.23	0.21
(4) Manual thresholding without illumination normalisation	78.94	20.91	0.15

Table 3-1 : The segmentation result for database 1

Table 3-1 represents segmentation result based on database 1. There are 36 PCB images in this database which contain 3840 sold joints altogether. In the first condition of experiment, 99.93% of solder joints are successfully detected with 0.07% of miss rate and 0% of false alarm rate. The second condition of experiment does not include the illumination normalisation step. The performance of segmentation slightly decreases to 99.70% in hit rate and slightly increases to 0.3% in miss rate. But the false rate remains the same with the test condition 1. In manual thresholding with illumination normalisation, 97.56% of hit rate, 2.23% of miss rate and 0.21% of false rate are achieved. Comparing the results for manual thresholding without illumination normalisation, it is clear that the detection rate decline to 78.94%, the miss rate and false rate increase to 20.91% and 0.15% respectively in test condition 4. Therefore, it is easy to see that the combination of automatic thresholding and illumination normalisation achieved the best result.

Condition of experiment	Hit rate (%)	Miss rate (%)	False rate (%)
(1).Automatic thresholding with illumination normalisation	99.83	0.17	0
(2) Automatic thresholding without illumination normalisation	99.03	0.64	0.24
(3) Manual thresholding with illumination normalisation	96.62	3.38	0
(4) Manual thresholding without illumination normalisation	81.64	18.04	0.32

Table 3-2 : The segmentation result for database 2

Table 3-2 represents segmentation result based on database 2. There are 38 PCB images in this database which contains 621 solder joints altogether. As in database 1, automatic thresholding with illumination normalisation achieved highest detection with 99.83% of hit rate, 0.17% of miss rate and 0% of false rate. Hit rate decreases to 99.03%, miss rate and false rate increase to 0.64% and 0.24% when illumination normalisation is removed from the experiment. In manual thresholding with illumination normalisation, 96.62% of hit rate, 3.38% of miss rate and 0% of

false rate are achieved. The correct detection rate is low for manual thresholding without illumination normalisation with 81.64% of hit rate, 18.04% of miss rate and 0.32% of false rate.

Since the acquisition system for database 1 and 2 are not the same, the detection results for both databases will be invariably different but are close all the same. In order to control the illumination condition in database 1, the acquisition system is covered with black screens that help to avoid external light sources. Database 2 is captured by normal digital camera under fluorescent light source in the lab. There are no special illumination systems or advanced X-Y position systems. From both databases, it can be clearly seen that illumination normalisation improves the segmentation in both automatic thresholding and manual thresholding. For database 1, the hit rate increases from 99.70% to 99.93% in automatic thresholding and the hit rate rises from 78.94% to 97.56% in manual thresholding. The segmentation result for database 2 also improves in the same way. The hit rate increases by 0.8% for automatic thresholding and 14.98% for manual thresholding.

Subsequently, the automatic thresholding is significantly involved in performance of detection of solder joint. For both database 1 and 2, the hit rate increases from 97.56% to 99.93% and from 96.62% to 99.83% when normalisation illumination is employed. Similarly, the hit rate increases from 78.94% to 99.7% and from 81.64% to 99.03% when normalisation illumination is not performed on solder joint image. As a result, the experimental results on these two databases show that segmentation performance can be significantly improved when both illumination and automatic thresholding are employed.

This research proposed a novel illumination normalisation approach for solder joint segmentation. Illumination variations under different lighting conditions can be significantly reduced by discarding low-frequency DCT coefficients. This approach has advantages in: 1) no modelling steps are required and 2) this approach is fast and it can be easily implemented in a real-time solder joint segmentation system. However, the shadowing and specularity problems have not been completely solved because they lie in the same frequency bands as some image features, the results show that this method can effectively eliminate the effect of uneven illumination and greatly improve the segmentation result.

3.9 Chapter Summary

This chapter proposes a computer vision system for the automatic detection, localisation, and segmentation of solder joints on Printed Circuit Boards (PCBs) under different illumination conditions. An illumination approach is applied to an image, which can effectively and efficiently eliminate the effect of uneven illumination while keeping the properties of image the same as in the corresponding image under normal lighting conditions. Consequently, special lighting and instrumental setup can be reduced in order to detect solder joints. These normalised images are insensitive to illumination variations and are used for the subsequent solder joint detection stages. In the segmentation approach, the PCB image is transformed from an *RGB* colour space to a *YIQ* colour space for the effective detection of solder joints from the background. The segmentation results show that the proposed approach improves the performance significantly for images under varying illumination conditions. The methodology presented in this chapter can be an effective method to reduce cost and improve quality in production of PCBs in the manufacturing industry.

Chapter 4

Classification of Solder Joints

4.1 Introduction

After segmentation of soldered regions, the next step of the inspection is to detect and locate any potential solder joint defects which will break down the functions of the PCBs products. Many research techniques have been developed to recognise faulty solder joints. Kim et.al. [7] used active lighting and a Multi Layer Perceptron network to classify 2D features and a Bayes classifier to classify 3D features. Other techniques include Artificial Neural Network (AAN) ensembles [33] which combine a genetic algorithm and AdaBoost algorithm to correct a former trained ANN's errors. Jiang et al. [36] introduced a simpler method to identify the positions of the solder joint and a tree structure classifier to categorize the defect of the solder joint. This methodology does not require special lighting or special equipment to capture the PCB image. Accianni et al. [31] extracted Wavelet coefficients and geometric parameters of the images and used a neural network system to characterise the solder joint defects on PCBs. To improve the recognition rate, Ong et al. [27] combined the orthogonal view and the oblique view at the pixel level with direct input to the ANN for processing. Although many methods have been developed in this area, these methods need a complex system of image acquisition. It is also important to select the right classification method to improve detection rate.

This chapter examines a new technique for solder joint defect classification using the Gabor filter which has been demonstrated to achieve high recognition rate and is resistant to misalignment [46]. This filter has also found favour in many

image processing fields due to its desirable characteristic of spatial locality and orientation selectivity. For this reason, the Log-Gabor feature has been chosen as a method for more accurately representing the shape information in solder joint image. Log-Gabor features have been heavily used in texture analysis [47]; expression characterisation [48, 49]; face recognition [46, 50]; eye location detection [51]; fabric defect detection [52]; fingerprint verification [53]; vehicle detection [54]; cell segmentation [55]; Script Identification [56]; edge detection [57] and iris recognition [58]. However, to the best of my knowledge, Gabor filters have not been applied to the solder joint classification.

Discrete Wavelet Transform (DWT) is also applied to extract feature vector from solder joint image. The advantage of wavelet is that it can be treated as image-to-image transformation. This will enable each wavelet coefficient to be treated as a pixel image and thus allows the image difference operation to be carried out [59]. In addition, Discrete Cosine Transform (DCT) has energy compaction property and good performance in illumination normalisation so DCT is also applied for feature extraction of solder joints.

Five different levels of solder joint quality in respect to the amount of solder pasted have been classified by using Mahalanobis Cosine distance measure. The experimental results are devoted to comparing the performance of the Log Gabor filter, DWT and DCT. The results prove that the Log-Gabor filter is the best compromise in term of correct classification percentage. In addition, the features used for diagnosis are evaluated without the knowledge of the industrial physical parameter process which is the advantage of using the Log Gabor filter in this research.

The remainder of this chapter is structured as follows. In the next section an overview of Gabor and Log Gabor Filter is provided and then followed by overview of DWT and DCT. The remaining sections present the experimental results, discussion and conclusion.

4.2 Gabor and Log Gabor Filters

In recent times, Gabor filters have emerged as one of the most commonly used techniques in the field of image recognition and analysis. An important property of

Gabor filters is that it has optimal localisation properties in both spatial and frequency domain [60] and can be used to decompose images into components corresponding to different scales and orientations. Gabor filters have Gaussian nature with a center frequency one orientation and two parameters of spatial expansion. A two-dimensional Gabor filter consists of a sinusoidal plane of particular frequency and orientation modulated by a two dimensional Gaussian envelope. A Gabor filter has the following form in the spatial domain:

$$g(x,y) = s(x,y)\,\omega_r(x,y), \tag{4.1}$$

where $s(x,y)$ is a complex sinusoidal carrier and $\omega_r(x,y)$ is the Gaussian envelope,

$$s(x,y) = e^{2\pi j[u_0 x + v_0 y]}, \tag{4.2}$$

$$\omega_r(x,y) = K\exp(-\pi(x_r^2 a^2 + y_r^2 b^2)), \tag{4.3}$$

where u_0 and v_0 are the spatial frequency of the sinusoidal and a and b are the sharpness of the Gaussian envelope. Also the orientation of the sinusoidal component to any angle φ by means of the rotation of the Gaussian about the origin is defined by

$$\begin{aligned} x_r &= x\cos(\varphi) + y\sin(\varphi) \\ y_r &= -x\sin(\varphi) + y\cos(\varphi) \end{aligned}. \tag{4.4}$$

The real and imaginary parts of typical 2D Gabor functions are shown is Figure 4.1and Figure 4.2

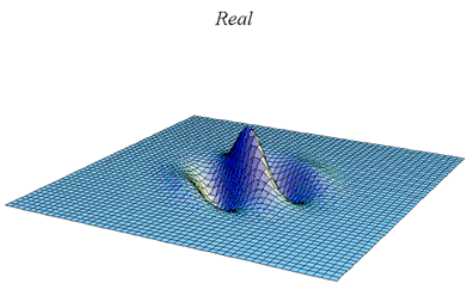

Figure 4.1 : The real part of a Gabor Filter [61]

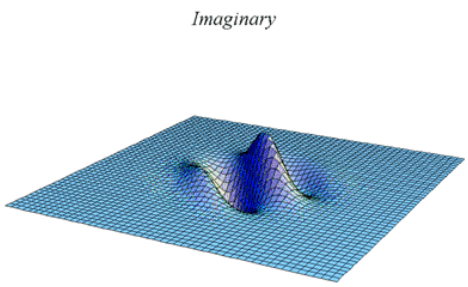

Figure 4.2 : The imaginary part of a Gabor Filter [61]

4.2.1 Gabor Filter Bank

The Gabor filter bank is a well known technique to determine a feature domain effectively for the representation of the images. The Gabor filter bank can be designed by varying spatial frequency and orientation of Gabor filters. The overall aim is to provide an even coverage of the frequency components of interest while maintaining a minimum of overlap between filters so as to achieve a measure of independence between the extracted coefficients [62].

4.2.2 Log Gabor Filters

However, Gabor filters can be designed for a bandwidth of 1 octave maximum and having small DC component in the filter. To overcome this limitation, Field [63] proposes Log-Gabor filters . Log-Gabor filters have no DC component and can be constructed with any arbitrary bandwidth. The frequency response of Log-Gabor filters are defined as

$$\Phi(\omega) = \exp - \frac{\ln(\omega / \omega_0)^2}{2\ln(\sigma / \omega_0)^2}, \qquad 4.5$$

where ω_0 is the centre frequency of the sinusoid and σ is a scaling factor of the bandwidth. Kovesi [64] suggests that in order to maintain constant shape ratio filters, the ratio σ / ω_0 should be maintained constant.

There are two important characteristics in Log-Gabor filters. Firstly Log-Gabor filter functions always have zero DC components which contribute to improve the contrast ridges and edges of images. Secondly, the Log-Gabor functions have an extended tail at the high frequency end which enables them to encode images more efficiently than ordinary Gabor function. The Log-Gabor filters have Gaussian transfer functions when viewed on a logarithmic frequency scale instead of on a linear one, an illustration of which can be seen in Figure 4.3. Log Gabor filters and Gabor filters have similar spatial characteristics for filters with low bandwidth (<1 octave) but appear much sharper.

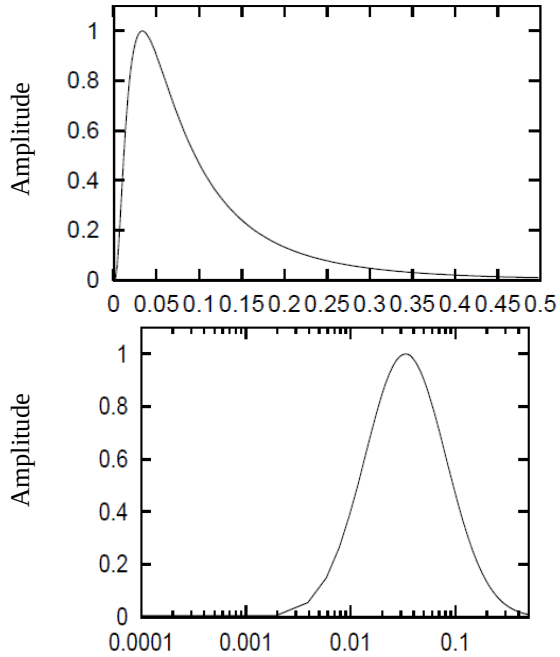

Figure 4.3 : An example of a Log Gabor transfer function viewed on both linear and logarithmic frequency scales [64]

In this experiment, the Log Gabor filter bank is constructed with a total of 6 orientations and 5 scales. The shape parameter, σ / ω_0 was chosen such that each filter had a bandwidth of approximately 1.5 octaves. The total of 30 feature vectors representing different scales and orientations are achieved.

4.3 Gabor Representation

Different combinations of Gabor representation are achieved from 30 feature vectors. The coefficients are complex by nature and can be represented by the features using:

- real component
- imaginary component
- real + imaginary component
- magnitude component
- phase component
- magnitude and phase component

However the magnitude representation outperforms all other single representations [62]. For remainder of the experimentation all coefficient are transformed to a purely magnitude based representation before further processing.

4.4 Discrete Wavelet Transform

The DWT is computed by successive low pass and high pass filtering of the discrete time-domain signal [65]. Wavelet decomposition is the projection onto an orthonormal set of basis vectors which are generated by dilation and translation of a single “mother wavelet”. In Figure 4.4, the signal is denoted by the signal X of length of N, the DWT consists of $\log_2 N$ levels at most. At each level, the high pass filter produces detail coefficients d[n], while the low pass filter associated with scaling function produces approximation coefficients a[n]. These vectors are obtained by convolving X with the low-pass filter Lo_D for approximation, and with the high-pass filter Hi_D for detail, followed by downsampling. At each decomposition level, the half band filters produce signals spanning only half the frequency band. This doubles the frequency resolution as the uncertainty in frequency is reduced by half.

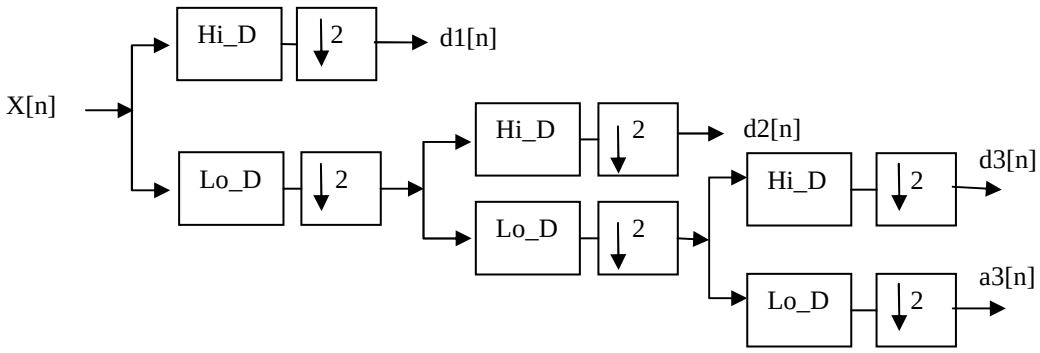

Figure 4.4 : Three level wavelet decomposition tree

There are a number of basis functions that can be used as the mother wavelet for Wavelet Transformation. Since the mother wavelet produces all wavelet functions used in the transformation through translation and scaling, it determines the characteristics of the resulting Wavelet transform. The simplest mother wavelet is the Haar wavelet,

$$\psi(t) = \begin{cases} 1 & : \quad 0 \le t < 1/2 \\ -1 & : \quad 1/2 \le t < 1 \\ 0 & : \quad else \end{cases}, \tag{4.6}$$

which generates the basic set,

$$\left\{ \psi_{j,n}(t) = \frac{1}{\sqrt{2^j}} \psi\left(\frac{t - 2^j n}{2^j} \right) \right\}_{(j,n) \in Z^2} . \tag{4.7}$$

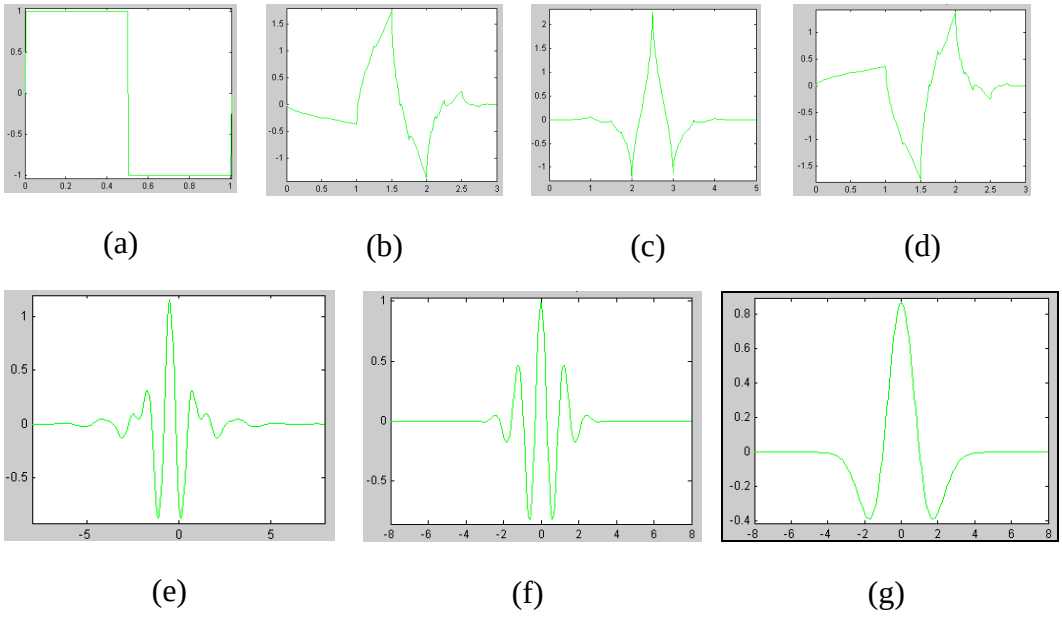

(a) (b) (c) (d)

(e) (f) (g)

Figure 4.5 : Wavelet families (a) Haar (b) Daubechies (c) Coiflet (d) Symlet (e) Meyer (f) Morlet (g) Mexican Hat

Figure 4.5 illustrates some of the commonly used wavelet functions. They represent the foundations of wavelet signal processing. The appropriate mother wavelet should be chosen based on their shape and their ability to analyse the signal in a particular application.

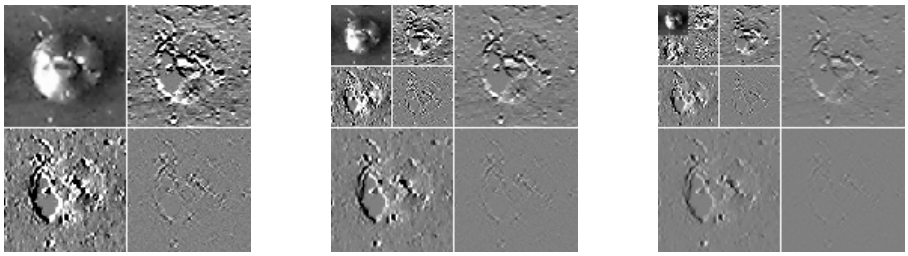

Figure 4.6 : First three levels of DWT using Haar wavelet (a) First level (b) Second level (c) Third level

Figure 4.6 illustrates the first three levels of 2D wavelet transform applied to good solder joint image. At each level the approximation of the previous level is split into horizontally, vertically and diagonally filtered images, known as detail coefficients and a subsequent approximation image. The wavelet filter bank can be formed by grouping together the detail coefficients at each level. In the following experimentation, 3 levels of decomposition are employed to achieve the equivalent of 4 filter banks.

4.5 Discrete Cosine Transform

DCT has been widely used in a feature extraction step and image compression because it has the effect of concentrating the energy in a signal in a relatively small number of coefficients [66]. The 2D-DCT is defined as

$$D(u,v) = \alpha(u)\alpha(v)\sum_{x=0}^{M-1}\sum_{y=0}^{N-1} f(x,y)\times\cos\left[\frac{\pi(2x+1)u}{2M}\right]\cos\left[\frac{\pi(2y+1)v}{2N}\right]. \qquad 4.8$$

In order to construct filter-banks from a DCT representation, the common overlapping block implementation, as is used in the Part-Face method of Lucey [67] and Sanderson [68], is utilised. A detected and normalised image is divided into blocks of $N \times N$ pixels size. In this experiment, M = N and $N = 8$. Each block, $f(x,y)$, where $x,y = 0,1, \ldots, N-1$, is decomposed in terms of pre-defined orthogonal 2D DCT basis functions as in Figure 4.7. The result is a $N \times N$ coefficient matrix $D(u,v)$:

where $u,v = 0,1,\ldots,N-1$, $\alpha(v) = 1/N$ for $v = 0$, $\alpha(v) = 2/N$ for $v = 1,2, \ldots, N-1$.

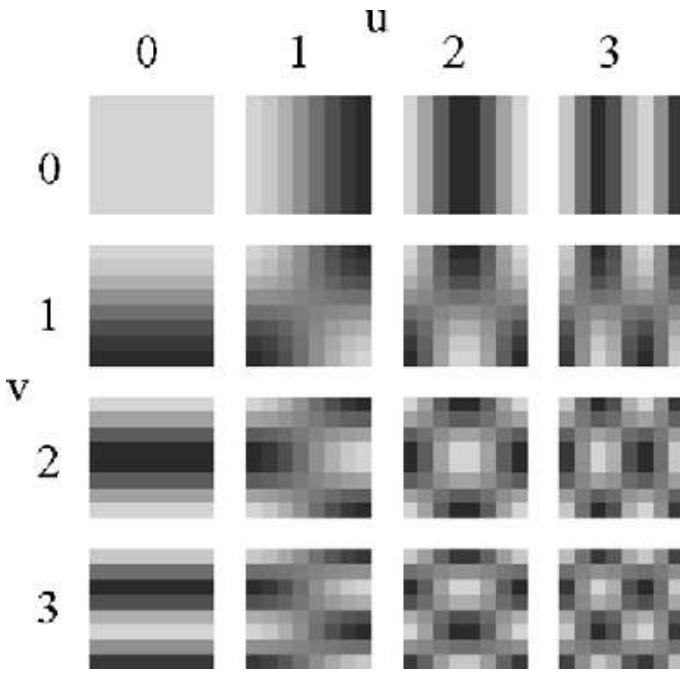

Figure 4.7 : Graphical interpretation of the first few 2D DCT basic function for N=8; (lighter colours represent larger value)

The top-left DCT coefficient is removed from the representation since it only represents the average intensity value of the block. From the remaining DCT coefficients the ones containing the highest information are extracted via zig-zag pattern as in Figure 4.8

	0	**1**	**2**	**3**
0	0	1	5	6
1	2	4	7	12
2	3	8	11	13
3	9	10	14	15

Figure 4.8 : Ordering of 2D DCT coefficients C *(v,u)* for $N_P = 4$

For block located at (b,a), the 2D DCT feature vector is composed of:

$$\vec{x} = [c_0^{(b,a)} \quad c_1^{(b,a)} \cdots c_{m-1}^{(b,a)}]^T, \tag{4.9}$$

where $c_n^{(b,a)}$ denotes the nth 2D DCT coefficient and m is the number of retained coefficients. To ensure adequate representation of the image, each block overlaps its horizontally and vertically neighbouring blocks by 50% [69]. Thus for an image which has N_Y rows and N_X columns, there are $N_D = (2(N_Y/N_P)-1) \times (2(N_X/N_P)-1)$ blocks.

4.6 Distance Measure

Mahalanobis Cosine distance is a distance measure between similarity of an unknown sample set to a known one. It takes into account the correlations of the data set and scale-invariant which is different from Euclidean distance. The transformation between the image space and the Mahalanobis space is needed to be performed before computing the Mahalanobis Cosine distance. Mahalanobis space is defined as a space where the sample variance along each dimension is one. To transform into Mahalanobis space, each coefficient in the image space feature vector is divided by its corresponding standard deviation. Let u and v be two vectors in the Eigenspace and σ is the standard deviation the ith dimension. Let m and n be the corresponding vectors in the Mahalanobis space. The relationship between the vectors is defined as

$$m_i = \frac{u_i}{\sigma_i} \quad and \quad n_i = \frac{v_i}{\sigma_i} \tag{4.10}$$

Mahalanobis Cosine Distance measure is the cosine of the angle between the projection of the images on the Mahalanobis space. So, for images u_i and v_i with corresponding projections m and n in Mahalanobis space, the Mahalanobis Cosine Distance is

$$D_{Mah\cos ine(u,v)} = -\frac{|m||n|\cos\theta_{mn}}{|m||n|} = -\frac{m \cdot n}{|m||n|} \quad . \tag{4.11}$$

4.7 The Detection Error Trade-off curve

The verification results are normally presented using Detection Error Trade-off (DET). The DET plot has a logarithmic scale on both axes which make it easier to observe the system contrast since the curves tend to be close to linear. The DET curve plot highlights the trade-off between false acceptance rate (false alarm probability) and false rejection rate (miss probability), which is useful in areas where trade-off between the two error types are important. The false acceptance rate is the measurement of the probability that a system will incorrectly indentify a solder joint class as another. The false rejection rate is the measurement of the probability that a system will fail to identify a solder joint class which is properly defined. There are a number of operating points on the curve which typically need to be considered in verification of the performance. The most common is the Equal Error Rate (EER). EER is the point at which the false alarm rate is equal to the miss probability rate. This may be used in applications to find the point of minimum cost in each type of error. The smaller the EER, the better. However, in general the whole DET curve is considered.

4.8 Experimentation and Result Analysis

Image database 3 is used to evaluate the classification algorithm. Database 1 and 2 are not used in this experiment since these do not include enough solder joint defects. The resolution of each solder joint image after segmentation is 40 x 40 pixels. Figure 4.9 shows the five different types of solder joints after segmentation. For each type of solder joint, 50 images are used as the training samples and two hundred images are used as the test samples. The images used for training and the testing sets have been chosen randomly from the original database for every individual experiment. During the test, experiments are performed 25 times and the

value averaged to get one complete classification result. When the number of experiments reached 25, the mean value became stable and this value was used to plot the graph. The experimental result is plotted as a probability distribution and evaluates the result by DET plot. From 1000 test images, the solder joints are classified into five different groups with respect to the amount of solder paste: good solder joint, excess solder joint, less (insufficient) solder joint, bridge solder joint and no solder joints. All the experiments and results are performed on the existing database and the result might be varied when this method is applied to an actual production environment. Other types of defects can be added to the system.

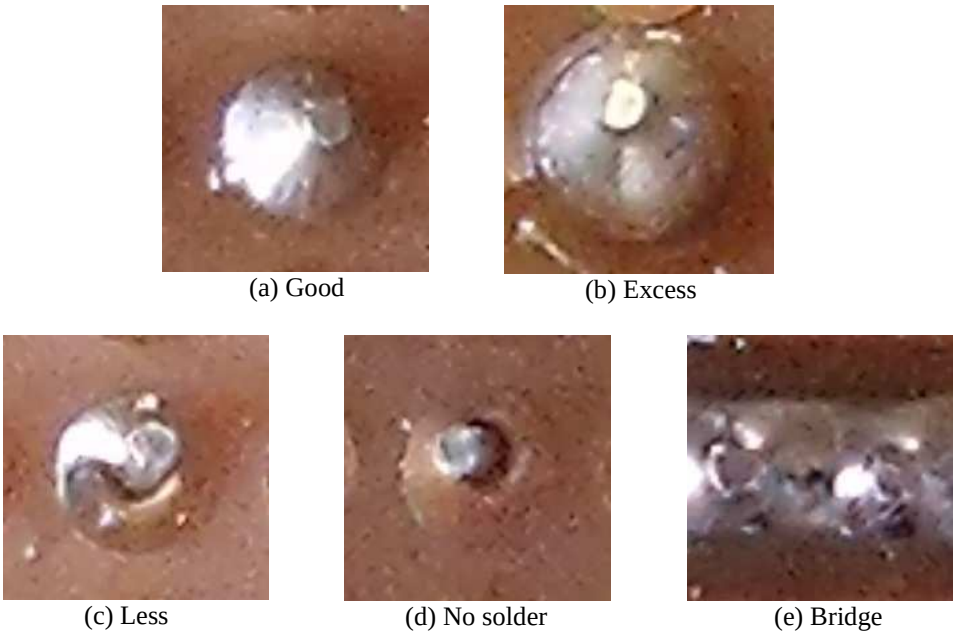

(a) Good (b) Excess

(c) Less (d) No solder (e) Bridge

Figure 4.9 : Different types of solder joint appearance

Table 4-1 represents the test scenarios and related figures for the experiments performed in this chapter. The experimental result and discussion for figures in second column of Table 4-1 presents in Section 4.8.1. Section 4.8.2 and Section 4.8.3 proposes the experimental result and discussion for figures in the third and forth column of Table 4-1 respectively. The experiments are performed within the available database.

Test condition	Log Gabor	Wavelet	DCT
scores of 200 good solder joints and scores of 800 defect solder joints (i.e., scores combination from excess, less, no joint and bridge) compare with scores of 50 training good solder joints	Figure 4.10 Figure 4.11	Figure 4.32 Figure 4.33	Figure 4.53 Figure 4.54
scores of 200 good solder joints and each scores of 200 defect solder joints (i.e., individual scores from excess, less, no joint and bridge) compare with scores of 50 training good solder joints	Figure 4.12 Figure 4.13	Figure 4.34 Figure 4.35	Figure 4.55 Figure 4.56
scores of 200 excess solder joints and scores of 600 defect solder joints (i.e. scores combination from less, no joint and bridge) compare with scores of 50 training excess solder joints	Figure 4.14 Figure 4.15	Figure 4.36 Figure 4.37	Figure 4.57 Figure 4.58
scores of 200 excess solder joints and each scores of 200 defect solder joints (i.e., individual scores from less, no joint and bridge) compare with scores of 50 training excess solder joints	Figure 4.16 Figure 4.17	Figure 4.38 Figure 4.39	Figure 4.59 Figure 4.60

Test condition	Log Gabor	Wavelet	DCT
scores of 200 less solder joints and scores of 600 defect solder joints (i.e. scores combination from excess, no joint and bridge) compare with scores of 50 training less solder joints	Figure 4.18 Figure 4.19	Figure 4.40 Figure 4.41	Figure 4.61 Figure 4.62
scores of 200 less solder joints and each scores of 200 defect solder joints (i.e., individual score from excess, no joint and bridge) compare with scores of 50 training less solder joints	Figure 4.20 Figure 4.21	Figure 4.42 Figure 4.43	Figure 4.63 Figure 4.64
scores of 200 no solder joints and scores of 600 defect solder joints (i.e. scores combination from excess, less and bridge) compare with scores of 50 training no solder joints	Figure 4.23 Figure 4.24	Figure 4.44 Figure 4.45	Figure 4.65 Figure 4.66
scores of 200 no solder joints and each scores of 200 defect solder joints (i.e., individual score from excess, less and bridge) compare with scores of 50 training no solder joints	Figure 4.25 Figure 4.26	Figure 4.46 Figure 4.47	Figure 4.67 Figure 4.68

Test condition	Log Gabor	Wavelet	DCT
scores of 200 bridge solder joints and scores of 600 defect solder joints (i.e., scores combination from excess, less and no joint) compare with scores of 50 training bridge solder joints	Figure 4.28 Figure 4.29	Figure 4.48 Figure 4.49	Figure 4.69 Figure 4.70
scores of 200 bridge solder joints and each scores of 200 defect solder joints (i.e., individual score from excess, less and no joint) compare with scores of 50 training bridge solder joints	Figure 4.30 Figure 4.31	Figure 4.50 Figure 4.51	Figure 4.71 Figure 4.72

Table 4-1 : Test Scenarios with corresponding figures

4.8.1 Gabor Filter

The Gabor and Log-Gabor filters are the closest in nature to the manner in which human's process visual stimulus [70] and there is no unique or ideal arrangement of the filters. The design of a filter bank is somewhat complicated and should consider some factors. One aspect of the filter-bank construction is to produce a filter bank that provides even coverage of the section of the spectrum that it wishes to represent. This can be achieved by making the overlap of the filter transfer functions sufficiently large in order to ensure full coverage. For computational reasons, the filter bank should be constructed with minimal overlap. Another aspect is to ensure the outputs of the individual filter in the bank are as independent as possible. To achieve independence of output, the filters should have minimal overlap of their transfer functions. Here are some parameters that should be considered in order to have the minimal overlap necessary to achieve even spectral coverage.

- The minimum and maximum frequencies
- The filter bandwidth

- The scaling between centre frequencies of successive filters
- The number of filter scales
- The number of filter orientations to use
- The angular spread of each filter

The maximum frequency is set by the wavelength of the smallest scale filter which is the Nyquist wavelength of 2 pixels. However, it is better to keep the minimum value to 3 pixels or above to avoid aliasing. The minimum frequency is set by the wavelength of the largest scale filter. This is simply defined after setting the number of filter scales (*nscale*) , the scaling between centre frequencies of successive filters (*multi*) and the wavelength of the smallest scale filter.

*maximum wavelength = minWavelength * mult^ (nscale -1)*

minimum frequency = 1/maximum wavelength

In the experiment, a bandwidth of 1.5 octaves gives the best feature extraction.

The scaling between centre frequencies of successive filters (*multi*) must also be determined to get the optimum result. This value is adjusted for the minimal overlap necessary to achieve fairly even spectral coverage. A scaling factor (*multi*) of 2.1 is applied for each subsequent filter, leading to frequency coverage of around 1.5 octaves which gives the best feature extraction.

The number of filter orientation, the angular spread of each filter, specifies the resolution of the orientation information from the filters. In this experiment, the images were convolved using the Log Gabor filter of 5 spatial frequencies and 6 orientations. Six angular orientations from 0 to 150 degrees in 30-degree steps are used.

Other important parameters for this filter included the ratio of the standard deviation of the Gaussian transfer function to the filter centre frequency (set to 6.5) and the ratio of the angular interval between filter orientation and the standard deviation of the angular Gaussian function (set to 1.5). The parameters for the filters were chosen by trial and error and are the common values that produce the best results.

The test scenarios for individual figure are described in Table 4-1

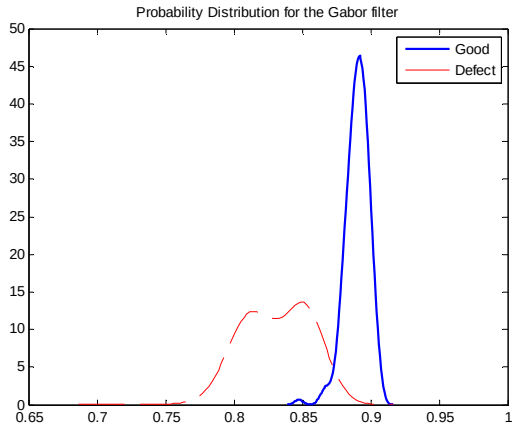

Figure 4.10: Probability distribution between good solder joints and defect solder joints

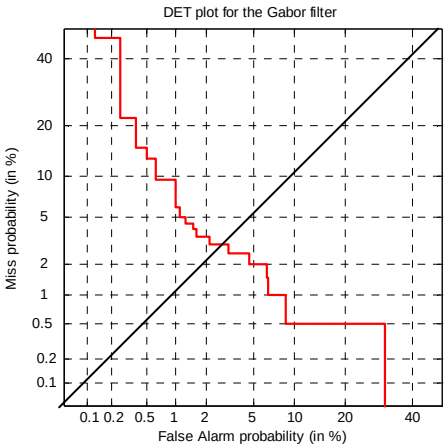

Figure 4.11: DET plot for classification performance of good solder joints and defect solder joints

In this experiment, there are 50 training samples and 200 testing samples for each type of joint. In Figure 4.10, the thick blue line represents the scores of 200 good testing samples compared to the scores of 50 good training samples. The red dash line represents the scores of 800 defect testing samples compared to the scores of 50 good training samples. The data is collected by performing experiments 25 times and plotting the average value in a probability distribution graph. The DET provides the function to support plotting the results of detection experiments in an intuitive meaningful way. Figure 4.11 is the DET plot which generates from the probability distribution of the good samples and defect samples from Figure 4.10. In Figure 4.11, EER is the point where the DET curve and diagonal line intersect. This figure achieves the EER of 3% which means the classification rate is 97%.

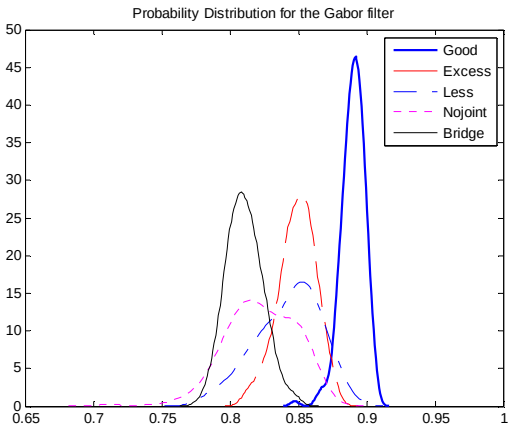

Figure 4.12: Probability distribution between good solder joints and individual defect solder joints

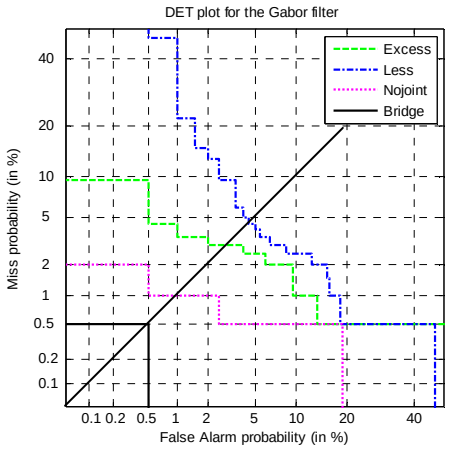

Figure 4.13: DET plot for classification performance of good solder joints and individual defect solder joints

In Figure 4.12, the thick blue line represents the scores of 200 good testing samples compared to the scores of 50 good training samples. The red dash line represents the scores of 200 excess joints compared to the scores of 50 good training samples and 3% of the EER is achieved from DET plot (Figure 4.13). Similarly, the blue dash line represents the scores of 200 less solder joints compared to the scores of 50 good training samples and 5% of the EER is achieved from DET plot (Figure 4.13).The same experiments are conducted to less, bridge and no solder joints. Gabor filter has a high detection rate for good solder joints and bridge solder joints with EER less than 1%. Less than 5% of the less solder joints are wrongly classified as good joint.

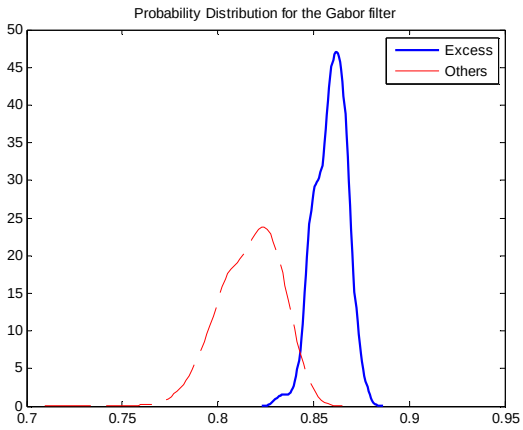

Figure 4.14: Probability distribution between excess solder joints and other defect solder joints

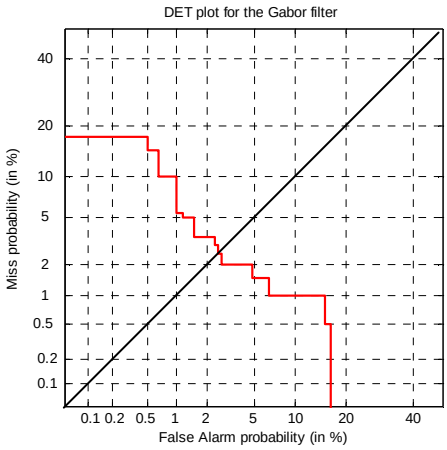

Figure 4.15: DET plot for classification performance of excess solder joints and defect solder joints

Figure 4.14 and Figure 4.15 show the probability distribution and DET plot for the excess joints and other defect joints. DET plot shows the EER rate of 3% which means the classification rate is 97%. Since good joints have been detected, it is not necessary to include classification of the individual defect types.

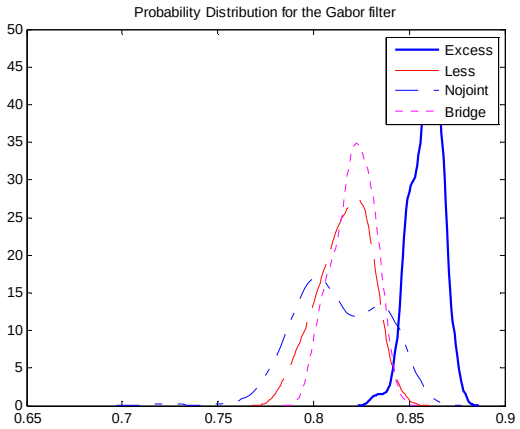

Figure 4.16: Probability distribution between excess solder joints and other individual defect solder joints

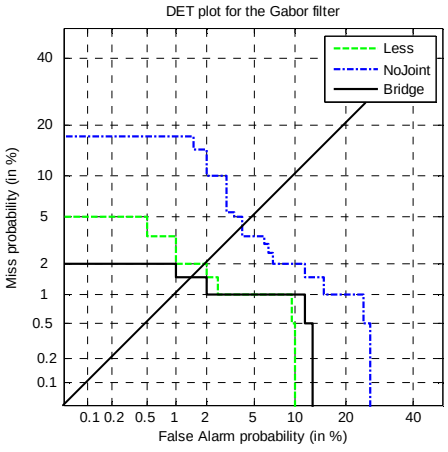

Figure 4.17: DET plot for classification performance of excess solder joints and other individual defect solder joints

Figure 4.16 and Figure 4.17 show the probability distribution and DET plot for excess joints and the other individual defect types (i.e., less, bridge and no solder

joint). Since good joints have been already detected, it is not necessary to include when classifying for the individual defect types. From the experimental results, the Gabor filter can highly classify excess joints with EER rate 2% for less solder joints, 4% for no solder joints and 1.5% for bridge solder joints.

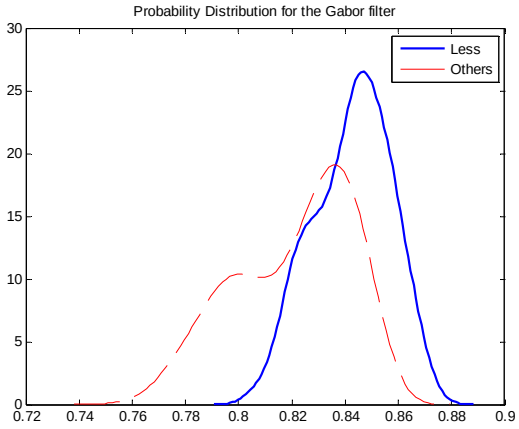

Figure 4.18: Probability distribution between less solder joints and other defect solder joints

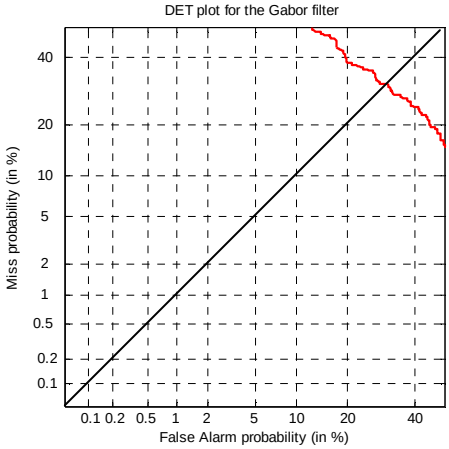

Figure 4.19: DET plot for classification performance of less solder joints and defect solder joints

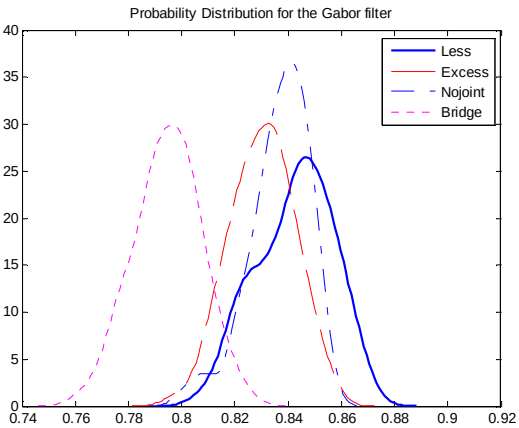

Figure 4.20: Probability distribution between less solder joints and other individual defect solder joints

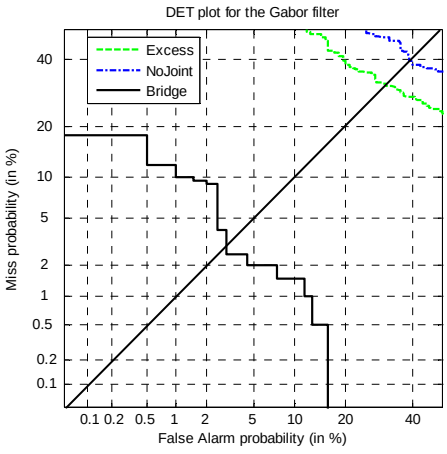

Figure 4.21: DET plot for classification performance of less solder joints and other individual defect solder joints

Figure 4.22: Different appearances of less (insufficient amount) of solder joints

From Figure 4.22, there is a high degree of difference between individual less solder joints which leads to poor classification results. The EER rate for the less joints with other defect solder joint is around 30%. In the same way, a high classification rate is not achieved for less solder joints compared to other defects. About 30% and 40% of excess solder joints and no solder joints are wrongly classified as less solder joint (Figure 4.21)

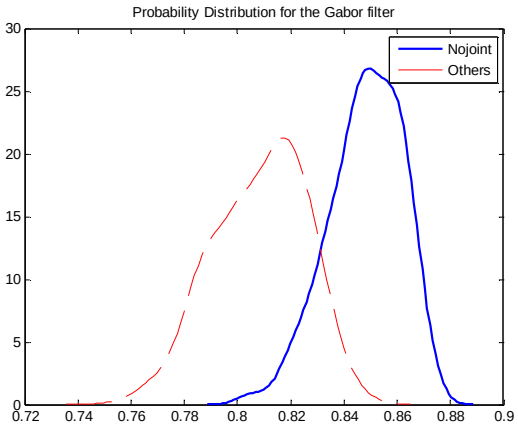

Figure 4.23: Probability distribution between no solder joints and other defect solder joints

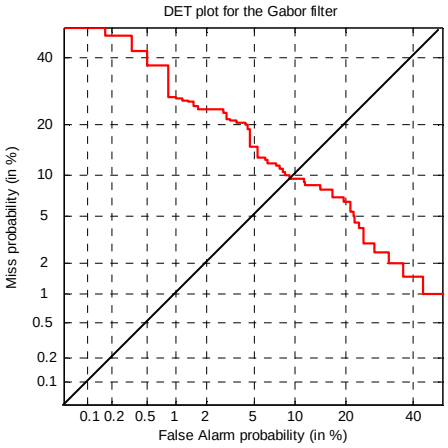

Figure 4.24: DET plot for classification performance of no solder joints and other defect solder joints

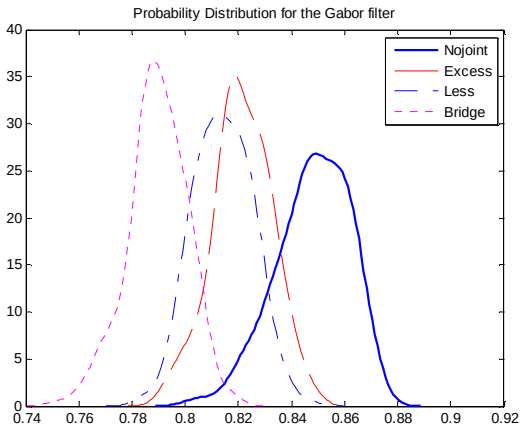

Figure 4.25: Probability distribution between no solder joints and other individual defect solder joints

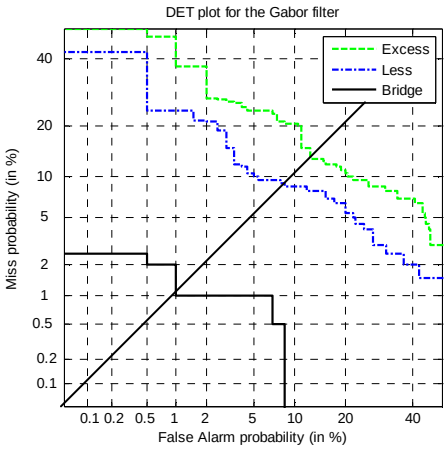

Figure 4.26: DET plot for classification performance of no solder joints and other individual defect solder joints

Figure 4.27: Different appearances of no solder joints

Similarly, from Figure 4.27, the lead direction of the components is not consistent in no solder joint which also leads to poor classification result. The EER for overall classification result is nearly 10% (Figure 4.24). About 9% of less solder joint and 14% of excess solder joint are incorrectly classified as no solder joint. Only 1% of bridge solder joint are wrongly classified so that the classification rate is quite high.

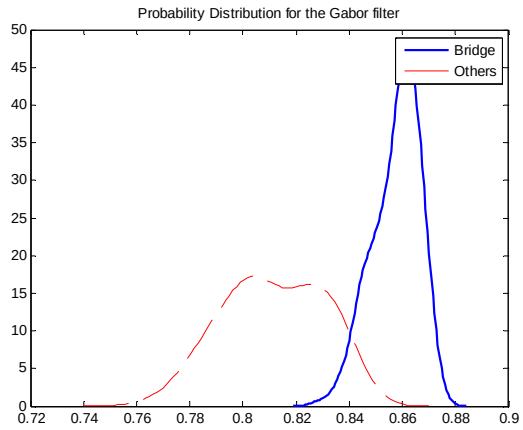

Figure 4.28: Probability distribution between bridge solder joints and other defect solder joints

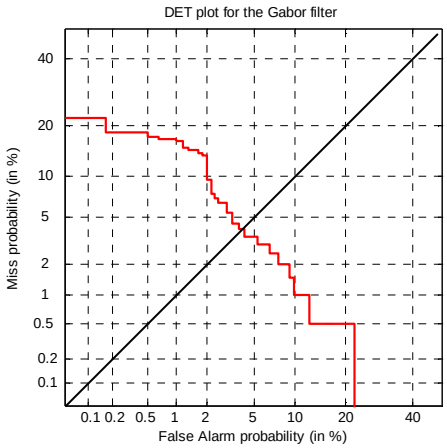

Figure 4.29: DET plot for classification performance bridge solder joints and other defect solder joints

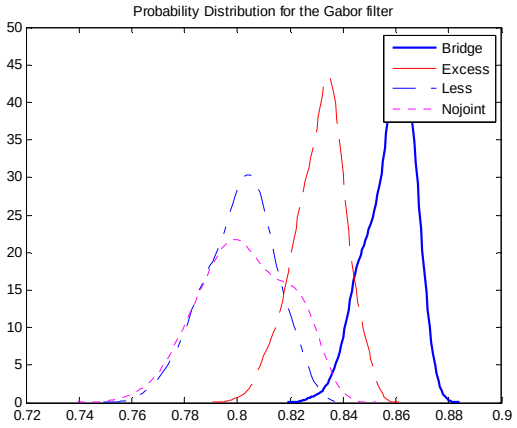

Figure 4.30: Probability distribution between bridge solder joints and other individual defect solder joints

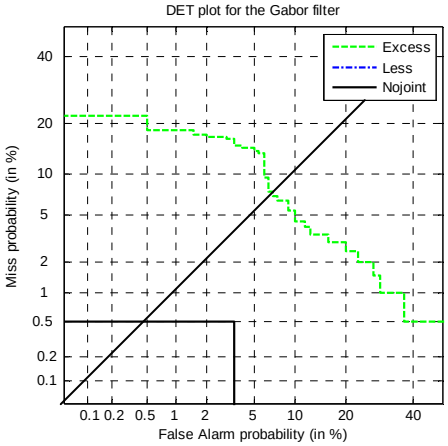

Figure 4.31: DET plot for classification performance of bridge joints and other individual defect joints

Since the overlap area between bridge solder joints and less solder joints is almost zero, it cannot be plotted on the DET and assumes that the EER is zero (Figure 4.31). From Figure 4.28 to Figure 4.31 represent the experimental result for bridge solder joints which achieve high performance in classification. The overall recognition rate for bridge solder joints is quite high and 4% of EER is achieved for bridge solder joints compared to other defects. The overall classification results from all DET plots are summarised in Table 4-2.

Solder Joint Types	Recognition rate and EER for Gabor filter				
	G	E	L	N	B
G (Good Joint)	**97**	3	4.5	1	0.5
E (Excess Joint)	-	**97**	2	4	1.5
L (Less Joint)	-	32	**60**	40	3.5
N (No Joint)	-	14	9	**90**	1
B (Bridge Joint)	-	7	0.5	0	**96.5**

Table 4-2 : Summary result for recognition rate of solder joints across five categories by using Log Gabor filter

A good classification algorithm will have a low percentage of false alarms and miss probability that is a small EER rate. In Table 4-2, the training samples are shown by column and the testing samples are shown by row.

The diagonal values across the table represent the recognition rate for classification of solder joints and the rest are EER. For example, from the reading across the first row and the first column, we see the percentage of good joints correctly classified was 97.0 %(Figure 4.11). Next column represents EER (3%) of excess solder joints classified as good solder joints. Since good joints have already been detected, it is not necessary to include them in the classification of the individual defect types. From Table 4-2, the recognition rates for good solder joints, excess solder joints and bridge solder joints are relatively high with about 97% which is followed by the recognition rate of no solder joint with 90%. About 60% of recognition rate is achieved for less solder joint. Less than 5% of EER is achieved for miss classification as good solder joint, excess solder joint and bridge solder joint as other defect types except for 7% of EER which is achieved from miss classification of excess solder joint as bridge solder joint which can be found in row 1(G), 2(E) and 5(B) of the table. EER is getting higher for miss classification as no solder joint and less solder joint. The highest EER is 40% for no solder joint incorrectly classified as less solder joints. The performance degradation due to the high degree of difference between individual less solder joints and some limitation of Gabor filter is mentioned below. The recognition performance can be improved by classifier fusion.

The proposed algorithm achieves preferable performance because the Gabor filter can capture visual properties such as spatial localisation, orientation selectivity, and spatial frequency characteristics. Log Gabor functions have no DC component, which contributes to the improvement of the contrast ridges and edges of images. Moreover, they have an extended tail at the high frequency end, which enables them to obtain wide spectral information with localised spatial extent and consequently helps to preserve true ridge structures of images. Because of the above characteristics, the Log Gabor filters give an average correct classification rate about 88%. Although the overall results are promising, the results presented in the table indicate that some deterioration of the recognition results is observed for the less and no solder joint defects because of the unstable surface of those defects.

The unstable surfaces are caused because of the following reasons in the Log-Gabor filter bank. In the Log-Gabor filter bank, its elementary functions overlap each other introducing coefficient redundancy between neighbouring coefficients. Due to non-orthogonality there is no straight forward method of finding the parameter values of the Gabor filter. The parameter values depend upon the surface (its orientation and frequency of repetition of the surface pixels) which is to be identified by a particular set of Gabor filters [71]. If any of these are affected due to different image degradation and the distortions of images, then the Gabor filter bank may not even work well.

In some cases, the Gabor filter bank cannot discriminate a certain image as a whole but rather certain frequencies from the image. This problem appears when image surfaces share the same frequencies or are comprised of close frequencies for certain orientations. These indicate that different feature selection strategies would have to be implemented to achieve a better classification result. As a result, DWT and DCT are studied to minimise the error in Log Gabor filter.

4.8.2 Discrete Wavelet Transform

Wavelet analysis has also been used to extensively provide a compact representation which separates the frequency content of a signal or image [66]. This property of wavelet is helpful to minimise the error in Gabor filter. The Discrete Wavelet Transform (DWT) is a dyadic multi-level transformation and provides a rigid partitioning of the frequency domain. At each level the frequency domain is

approximately split in two by the high-pass and low-pass filters. The center frequencies of the DWT can be estimated by assuming that each iteration cuts the frequency domain into two equal sized regions.

In the following experiment, all the frequency measurements are given on the normalised frequency scale where $f_{sampling}$ = 1Hz. The highest frequency which can be represented in this scale thus has a normalised value of 0.5Hz according to Nyquist's sampling theory. Assume that each level approximately halves the frequency domain and that the upper half is used to generate the detail coefficients. Given this, the detail coefficients encompass information from the range [0.25, 0.5] Hz and the center frequency of this would then be 0.375 Hz. The second level would encode the frequency range [0.125, 0.25] and have a centre frequency of 0.1875, subsequent levels would have center frequencies which decrease in a similarly dyadic manner.

These wavelets have the advantage of giving better resolution for smoothly changing time series. One of the principal benefits of the wavelet transform is the ability to capture transient phenomena, as the wavelet order increases so too does the sharpness and accuracy of the filter [66]. However, the sharpness of these filters against the smoothly changing nature of solder joint images means it becomes obvious that it is more appropriate to use the smoother lower order wavelet. There are many popular wavelet families being used in different applications such as Daubechies and Coiflet wavelets. The EER of the Daubechies wavelet transform (level 2) is 5% and EER of the Daubechies wavelet (level 4) is slightly more than 5%. However, they have the disadvantage of being more computationally expensive than the Haar wavelets. The Haar wavelet transform has a number of advantages [72]:

- It is conceptually simple.
- It is fast.
- It is memory efficient, since it can be calculated in place without a temporary array.

In this experiment, Haar wavelet gives the best performance across all images if compared to other wavelet families. The test scenarios from Figure 4.32 to Figure 4.51 are described in Table 4-1 column 3.

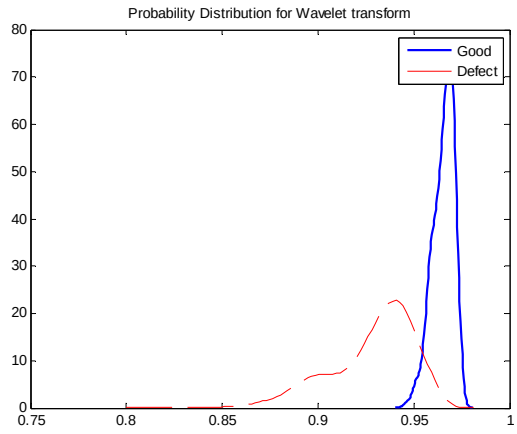

Figure 4.32: Probability distribution between good solder joints and defect solder joints

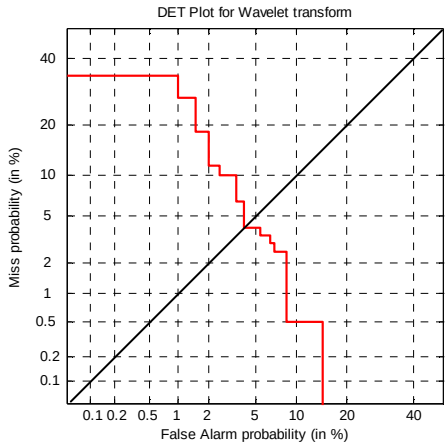

Figure 4.33: DET plot for classification performance of good solder joints and defect solder joints

Figure 4.32 and Figure 4.33 represent the overall classification rate of good solder joints compared to defect solder joints. About 5% of EER is achieved which is slightly higher than the EER rate of the Gabor filter. The following figures show experimental results for classification of solder joints by using DWT. The results are summarised in Table 4-3.

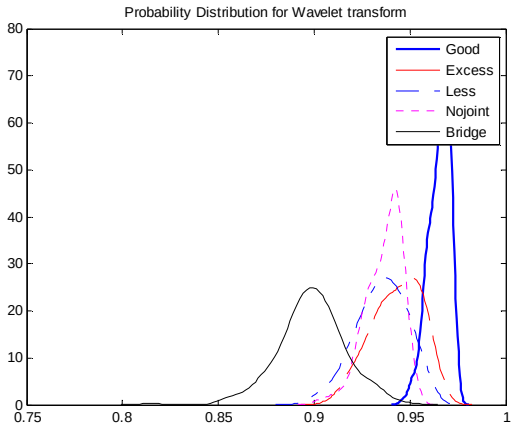

Figure 4.34: Probability distribution between good solder joints and individual defect solder joints

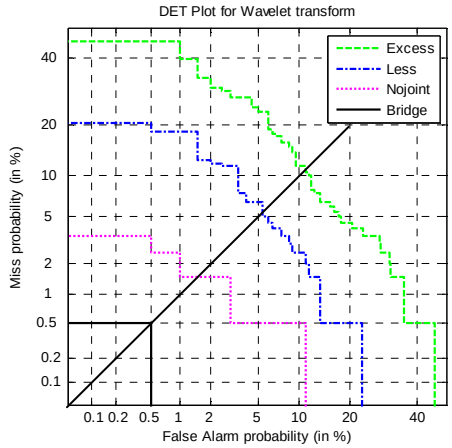

Figure 4.35: DET plot for classification performance of good solder joints and individual defect solder joints

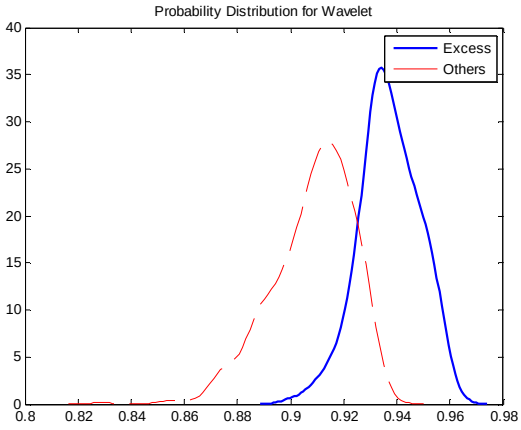

Figure 4.36: Probability distribution between excess solder joints and other defect solder joints

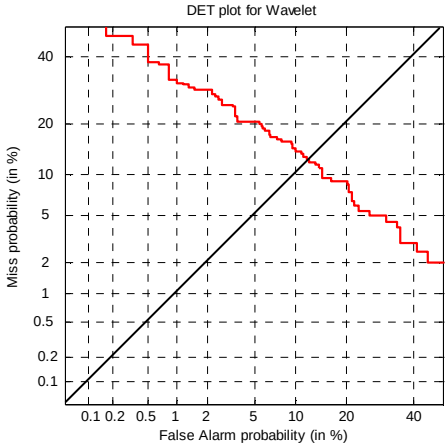

Figure 4.37: DET plot for classification performance of excess solder joints and other defect solder joints

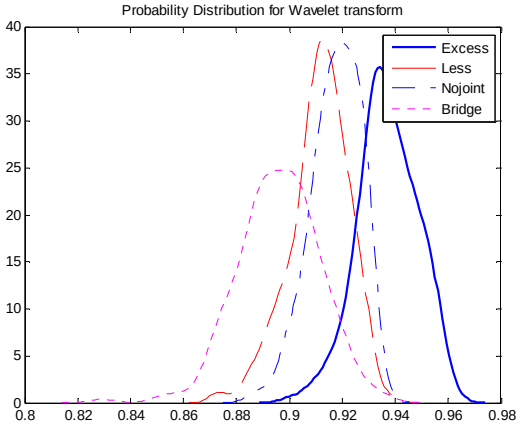

Figure 4.38: Probability distribution between excess solder joints and other individual defect solder joint

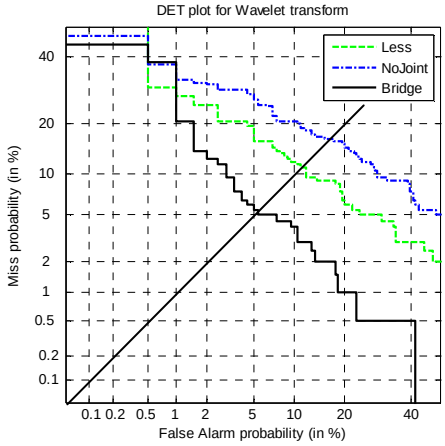

Figure 4.39: DET plot for classification performance of excess solder joints and other individual defect joints

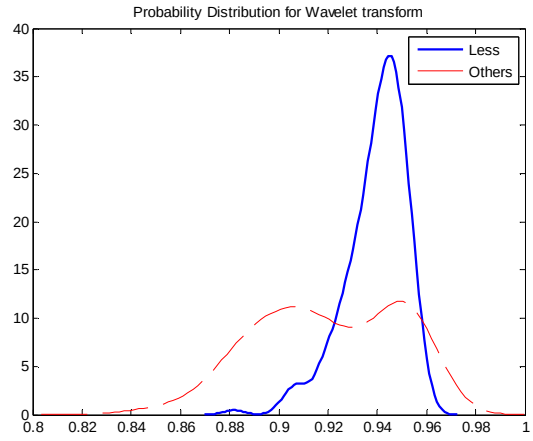

Figure 4.40: Probability distribution between less solder joints and other defect solder joints

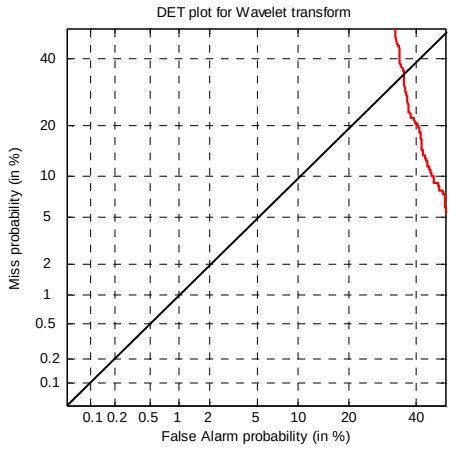

Figure 4.41: DET plot for classification performance of less solder joints and defect solder joints

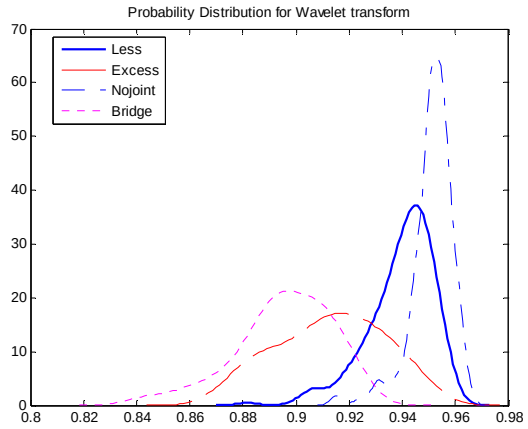

Figure 4.42: Probability distribution between less solder joints and other individual defect solder joints

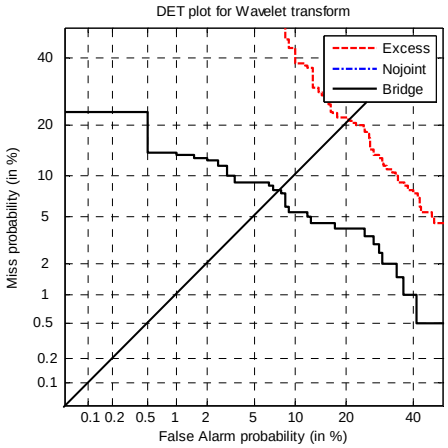

Figure 4.43: DET plot for classification performance of less solder joints and other individual defect solder joints

Since the overlap area between less solder joint and no solder joint is large, it cannot be plotted on the DET and assumes that the EER is over 40 (Figure 4.43).

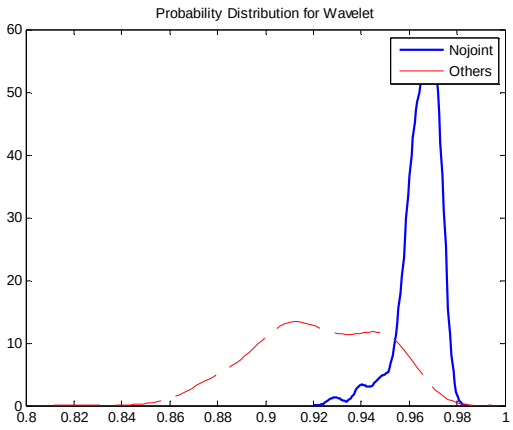

Figure 4.44: Probability distribution between no solder joints and other defect solder joints

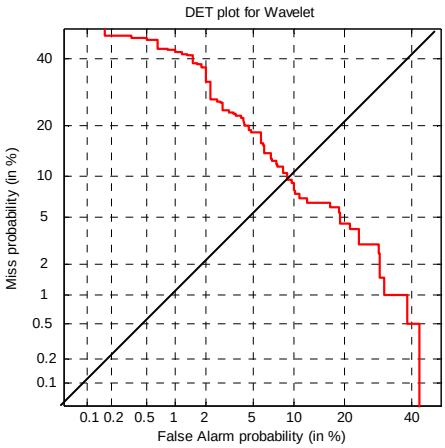

Figure 4.45: DET plot for classification performance of no solder joints and defect solder joints

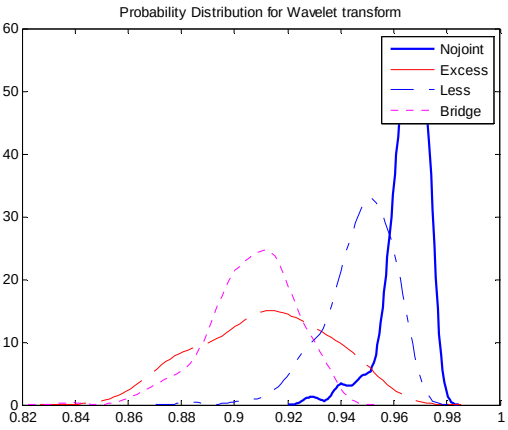

Figure 4.46: Probability distribution between no solder solder joints and other individual solder defect joints

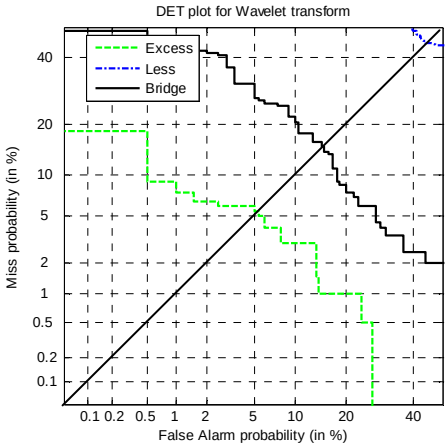

Figure 4.47: DET plot for classification performance of no solder joints and other individual solder defect joints

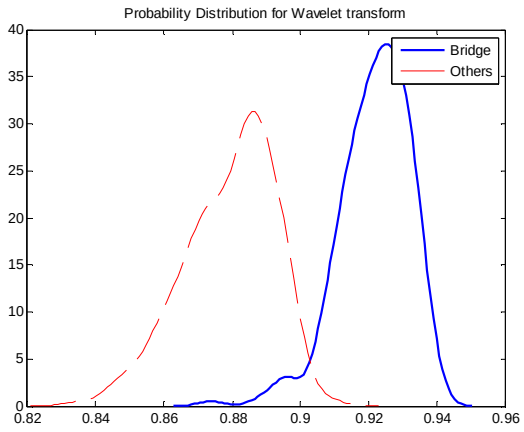

Figure 4.48: Probability distribution between bridge solder joints and other defect solder joints

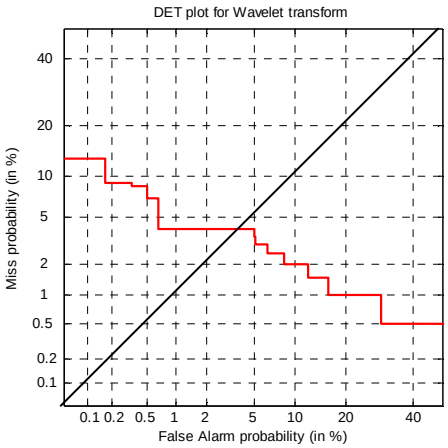

Figure 4.49: DET plot for classification performance of bridge solder joints and defect solder joints

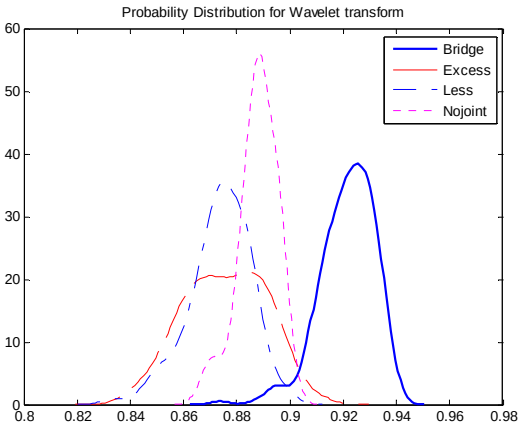

Figure 4.50: Probability distribution between bridge solder joints and other individual defect solder joints

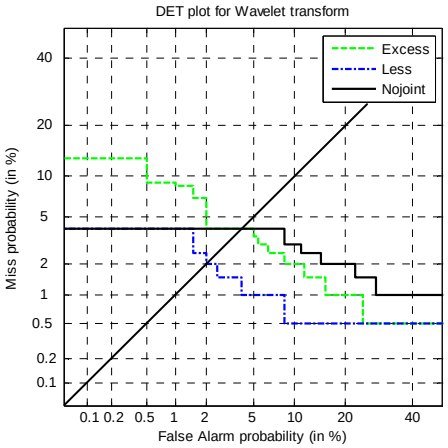

Figure 4.51: DET plot for classification performance of bridge solder joints and other individual defect solder joints

Solder Joint Types	Recognition rate and ERR for Wavelet Transform				
	G	E	L	N	B
G (Good Joint)	**96**	10	5	1.5	0.5
E (Excess Joint)	-	**86**	12	16	5
L (Less Joint)	-	20	**65**	>40	8
N (No Joint)	-	5	>40	**90**	16
B (Bridge Joint)	-	4	2	4	**96**

Table 4-3 : Summary result for recognition rate of solder joints across five categories by using Wavelet Transform

In Table 4-3, the diagonal values across the table represent the recognition rate for each type of solder joint and the rest present EER. The 96% of good joints is correctly classified which is the same as the percentage of bridge solder joint correctly classified. It is followed by the percent of correct classification of no solder joint and excess joint with 90% and 86% respectively. Only 65% of less solder joint are correctly classified. The average percentage of the correct classifications varied across different types from 96% to 65% whereas the DWT yields an average correct classification rate about 86%.

Although the overall recognition rate is not achieved as high as the Log Gabor filter, DWT perform well in less solder joint defects where recognition rates increase by 5% compared to the Log Gabor filter. The EERs of less solder joint classified as no solder joint and no solder joint classified as less solder joint are about 40% due to the high degree of difference between each solder joint (Figure 4.22) and the limitation of the Haar wavelet transform.

Since the Haar wavelet transform performs an average and difference on a pair of values and then shifts over by two values and calculates another average and difference on the next pair, it cannot detect if a big change takes place from an odd index value to an even index value [72]. For example, for a one dimensional signal that has 24 elements as shown in Figure 4.52, there is a large drop between elements 6 and 7, and a large rise between elements 11 and 12. After the first stage of wavelet transform, results for the high frequency computation is shown in Figure 4.52 as well. Only the large drop between elements 6 and 7 is detected in Figure 4.52_d1. Large rise between elements 11 and 12 is not detected because the change is from an odd element to an even element. For this reason, the performance degradation is caused for certain types of images like less solder joints.

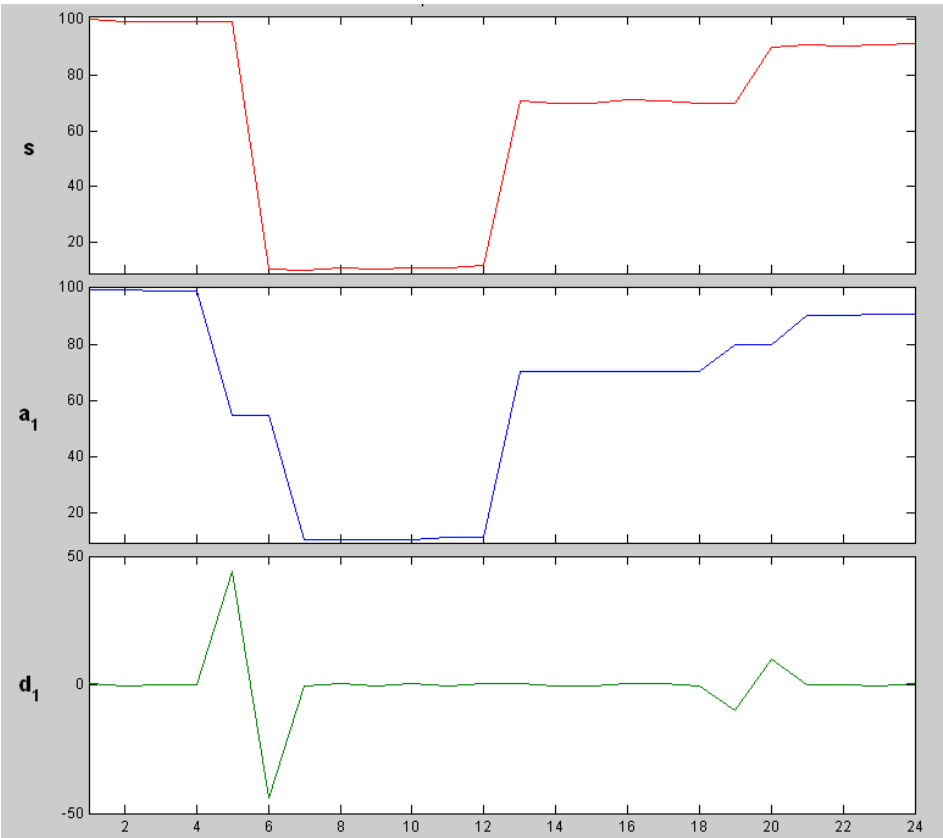

Figure 4.52: One-dimensional signal with a large drop between elements 6 & 7 and a large rise between elements 11 &12

4.8.3 Discrete Cosine Transform

There are several advantages of using the DCT in image processing application. The first advantage of the DCT is its efficiency. In transforming to the frequency domain, the Blocked DCT is used, which performs the same task as Fast Fourier Transform (FFT) in a more efficient manner. However, computing a blocked DCT does not actually require manual separation of the image into blocked, but rather this blocking occurs as an inherent function of the DCT.

Another advantage of the DCT is that its basis vectors are comprised of entirely real-valued components. Therefore all pixel values are represented by real numbers and the pixels themselves do not affect each other as values of the pixels come directly from the transform of the time domain values.

The block based nature of the DCT makes exact comparisons with the DWT and Gabor filters difficult. To make the comparison as equal as possible a range of block sizes are considered providing differing levels of spatial locality to the extracted features. By overlapping the blocks used for extraction it is less likely that

discriminative features will be excluded from the representation but at the cost of introducing redundancy. In this experiment, a 50% overlapping block approach was conducted and the results are displayed in the following figures.

The test scenarios from Figure 4.53 to Figure 4.72 are described in Table 4-1. These figures show experimental results for classification of solder joints by using DCT and all the results are summarised in Table 4-3

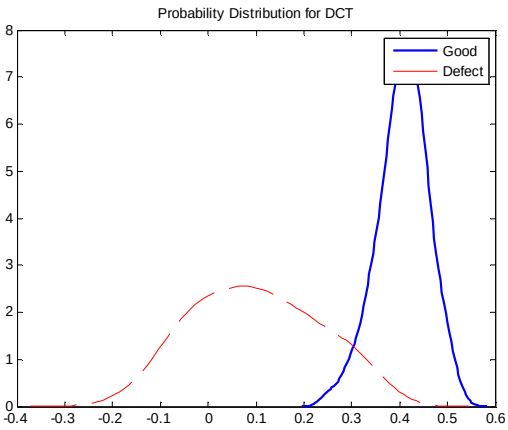

Figure 4.53: Probability distribution between good solder joints and defect solder joints

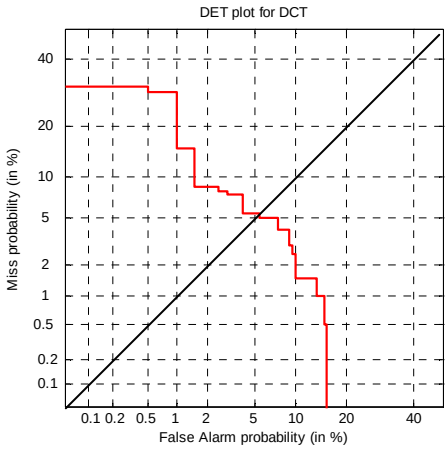

Figure 4.54: DET plot for classification performance of good solder joints and defect solder joints

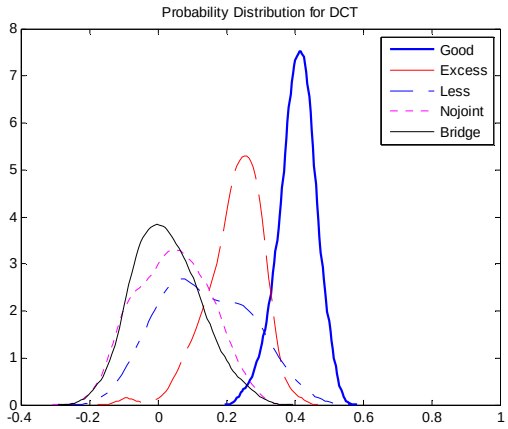

Figure 4.55: Probability distribution between good solder joints and other individual defect solder joints

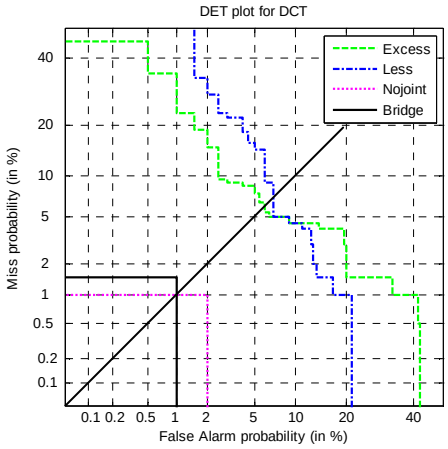

Figure 4.56: DET plot for classification performance of good solder and other individual defect solder joints

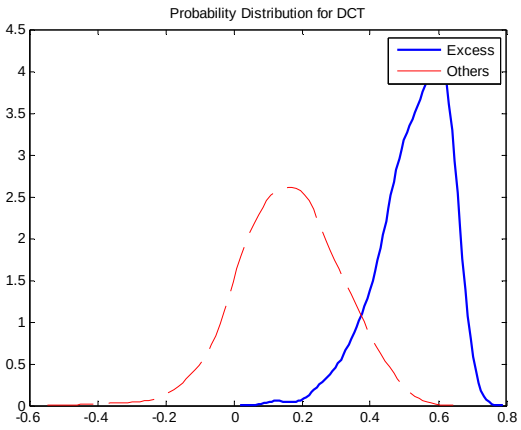

Figure 4.57: Probability distribution between excess solder joints and other defect solder joints

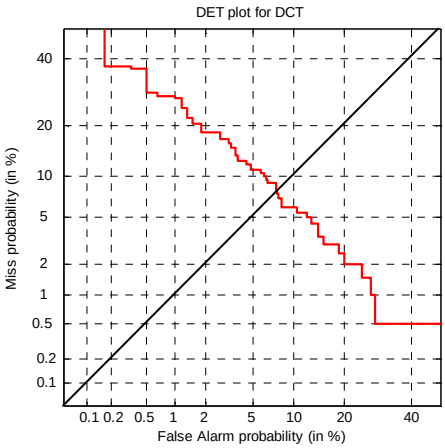

Figure 4.58: DET plot for classification performance of excess solder joints and other defect solder joints

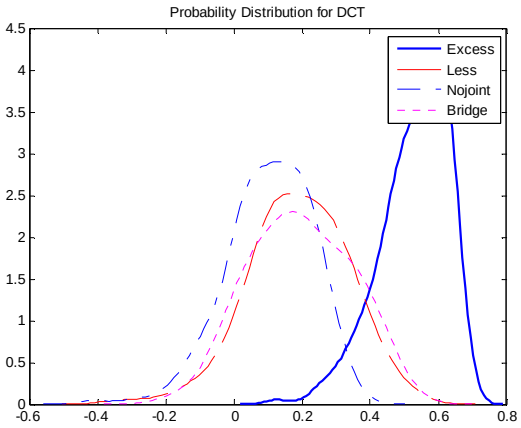

Figure 4.59: Probability distribution between excess solder joints and other individual defect solder joints

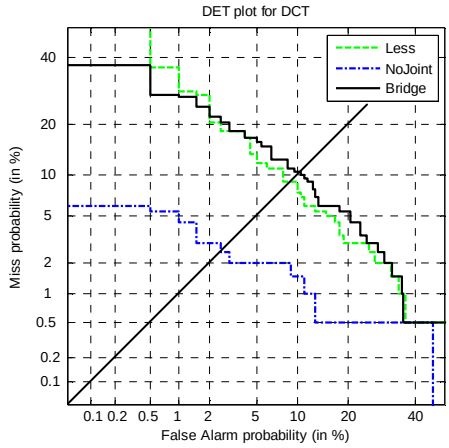

Figure 4.60: DET plot for classification performance of excess solder joints and other individual defect solder joints

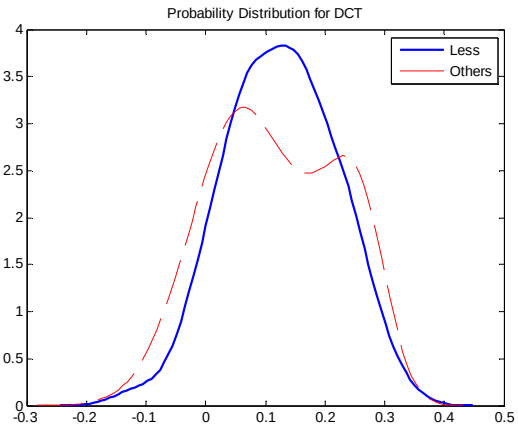

Figure 4.61: Probability distribution between less solder joints and other defect solder joints

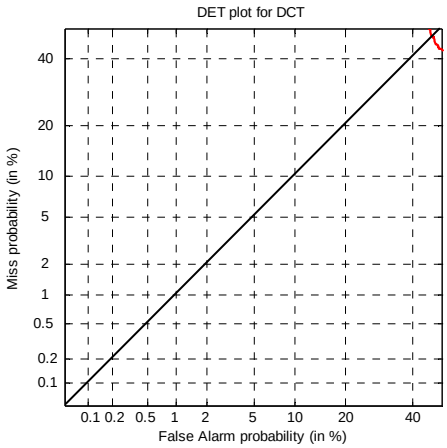

Figure 4.62: DET plot for classification performance of less solder joints and other defect solder joints

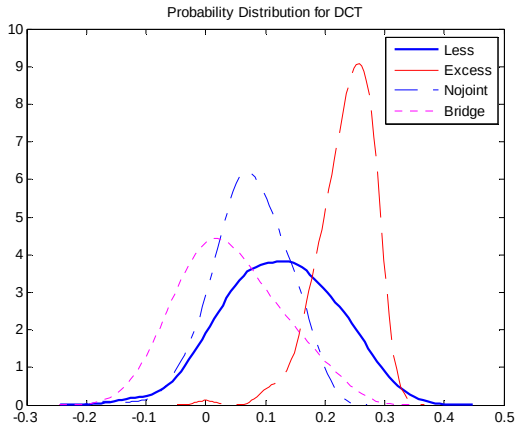

Figure 4.63: Probability distribution between less solder joints and other individual defect solder joints

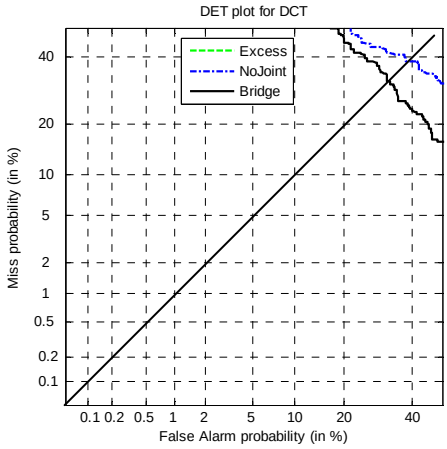

Figure 4.64: DET plot for classification performance of less solder joints and other individual defect solder joints

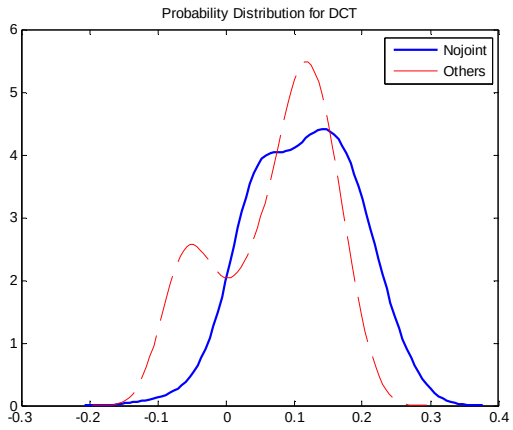

Figure 4.65: Probability distribution between no solder joints and other defect solder joints

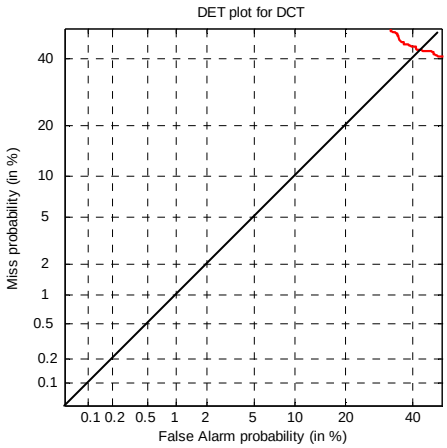

Figure 4.66: DET plot for classification performance of no solder joints and defect solder joints

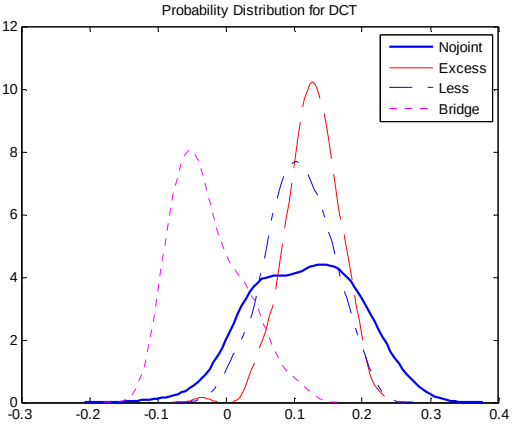

Figure 4.67: Probability distribution between no solder joints and other individual defect solder joints

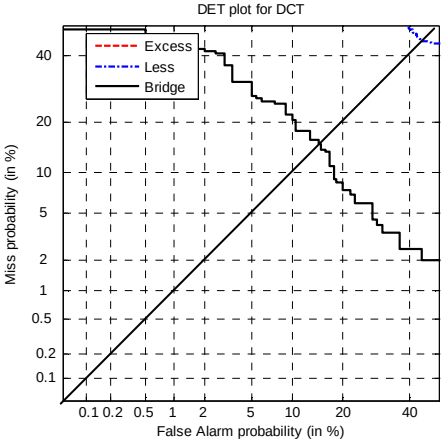

Figure 4.68: DET plot for classification performance of no solder joints and other individual defect solder joints

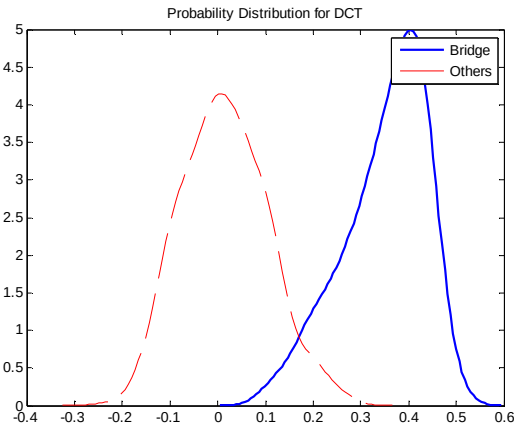

Figure 4.69: Probability distribution between bridge solder joints and other defect solder joints

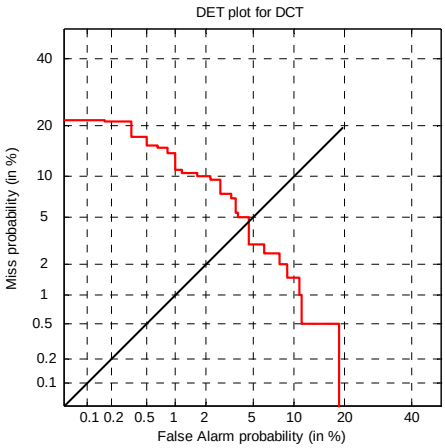

Figure 4.70: DET plot for classification performance of bridge solder joints and other defect solder joints

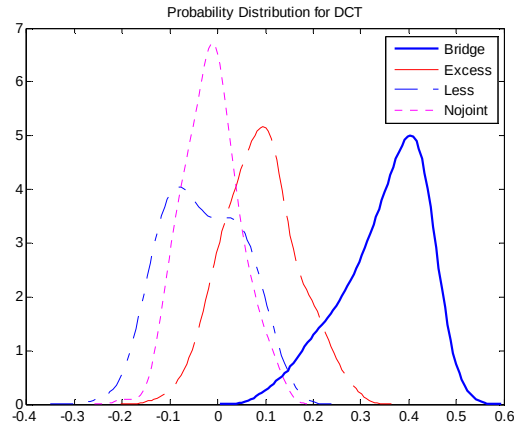

Figure 4.71: Probability distribution between bridge solder joints and other individual defect solder joints

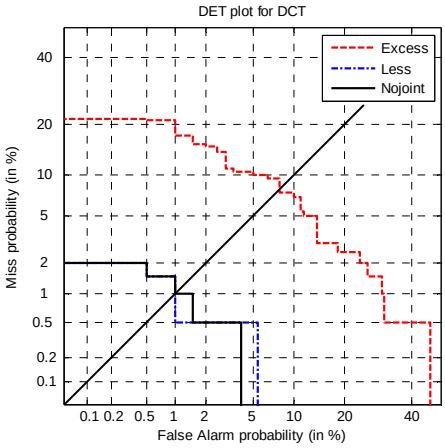

Figure 4.72: DET plot for classification performance of bridge solder joints and other individual defect solder joints

Solder Joint Types	Recognition rate and ERR for Discrete Cosine Transform				
	G	E	L	N	B
G (Good Joint)	**95**	7	8	1	1
E (Excess Joint)	-	**93**	9	3	10
L (Less Joint)	-	>40	**<60**	40	33
N (No Joint)	-	>40	>40	**<60**	15
B (Bridge Joint)	-	7	1	1	**95**

Table 4-4 : Summary result for recognition rate of solder joints across five categories by using Discrete Cosine Transform

In Table 4-4, the diagonal values across the table represent the recognition rate for each type of solder joint and the rest present EER. The number of good joints and bridge joints correctly classified is 95%, the number of excess joints classified as good joint is 7%, the number of less joints classified as good joint is 8% and so on. Similarly, the number of excess joints correctly classified is 93%. The average percentage of the correct classifications varied across different types from 95% to 60%. An average correct classification rate achieved by using DCT is 80.6%. Although the overall recognition rate is not achieved as high as the Log Gabor filter, DCT is evaluated as a method for utilisation in classifier fusion. From the experimental results, the Log Gabor representation out performs both the DWT and DCT representations and can be fused together to obtain desirable characteristics of them.

The recognition rate of less and no solder joints achieves around 60% due to the high degree of difference between each solder joint (Figure 4.22 and Figure 4.27) and limitation of DCT. The blockwise DCT destroys the invariance properties of the system, because the blockwise frequencies do not produce a simple relation to the frequencies achieved by just transforming the image into the frequency domain. Hence, any linear scaling factor from the time domain will not carry over into the frequency domain if blocking is used because linearity is no longer maintained. For this reason, the performance degradation is caused for certain types of images like less solder joints and no solder joints.

4.9 Summary

In this chapter, three techniques for the classification of solder joint defects are identified and tested using database 3. Gabor filter bank is proposed for feature extraction of solder joint images on PCBs. A distance measure based on the Mahalanobis Cosine metric is also presented for classification of five different types of solder joints. The classification correctness is evaluated by Detection Error Tradeoff (DET) curves and the recognition rate reaches 98%.

The wavelet transform uses more coefficients to represent high-frequency content and less coefficients for low frequency content. This causes the available

information concentrates at each scale level, which improves the performance of the tested classifier. The recognition rate for this technique is 95%.

2D Discrete Cosine Transform is also investigated for feature extraction techniques in order to counteract the effects of linear and non-linear illumination changes. The 2D DCT with a block size of 8 x 8 is preferred due to its lower computational complexity. Removing the first coefficient, which is most affected by illumination changes, clearly enhances robustness which have achieved the EER of 5%. However, removing further coefficient causes a noticeable reduction in performance on clean images.

From the experimental results, a bank of Log-Gabor filters has been shown to outperform DWT and DCT. In the next chapter, a method for combining the information from the above three techniques is examined and is known as classifier fusion. Classifier fusion aims to improve the accuracy and robustness of a classification system by combining multiple sources of information.

Chapter 5

Classifier Fusion

In Chapter 4, it is shown that effective classification of solder joints can be performed using the Gabor filter, the Wavelet transform and Discrete Cosine Transform. In this chapter, a method for combining the information from these classification systems is examined. Fused classification aims to improve the accuracy and robustness of a classification system by combining multiples sources of information. These information sources need to be complementary as redundant information will not improve verification. Classifier fusion combines the information from multiple verification systems that are achieved from three different classifiers. The advantage of the linear classifier fusion technique is that complex data and feature normalisation methods do not need to be employed.

5.1 Linear Classifier Score Fusion

This chapter aims to improve solder joint classification by performing linear classifier score fusion. Linear classifier score fusion is chosen as it has been shown to be robust to estimation error. [73]. A weighted linear fusion (where the optimal weights are found) using a linear logistic regression (*llr*) is employed in this research. The weighted fusion is of the form

$$C_{Weight\_sum} = \sum_{k=1}^{M} \beta_k C_k \ , \qquad 5.1$$

where β_k is the weight given to the k^{th} classifier C_k. Weighted linear fusion introduces a Z-score normalisation step to improve the generalisability of the technique. Z-score normalisation sets the mean and standard deviation of the score distribution to zero and unity respectively. The normalisation provides a consistent frame of reference from which the scores can be fused and is made under the assumption that the scores are normally distributed. The scores with the same range of magnitude are achieved as the outputs of the normalisation. Two properties of Z-score normalisation are:

- the resultant client scores are displaced further from the imposter scores and
- there will be a reduction in the variance of the combined imposter scores.

Z-scored normalisation is performed before linear logistic regression (*llr*) algorithms are applied to provide a consistent frame of reference between the weights being derived.

The *llr* is chosen in this thesis because it has a convex cost function and so will converge to a solution. The cost functions for the *llr* make use of the logit function. The logit function is defined as

$$\text{logit } P = \log \frac{P}{1-P}, \tag{5.2}$$

The cost function of the *llr* is as followed

$$C_{llr} = \frac{P}{K}\sum_{j=1}^{K}(1+e^{-f_j-\text{logit } P}) + \frac{1-P}{L}\sum_{j=1}^{L}\log(1+e^{g_j+\text{logit } P}). \tag{5.3}$$

For this cost functions K is the number of true trials, L is the number of false trials, P is the synthetic prior (which by default is P=0.5) and the fused target and non-target scores are respectively;

$$f_j = \alpha_0 + \sum_{i=1}^{N}\chi_i s_{ij} \quad and \quad g_j = \alpha_0 + \sum_{i=1}^{N}\chi_i r_{ij}. \tag{5.4}$$

A package provided by Brummer [74] is utilised for the implementation of this score fusion and the results of fusing the three classifiers together is provided in the following from Figure 5.1 to Figure 5.10.

5.2 Experimental Results and Analysis

To demonstrate the recognition ability of this technique, the classification results are plotted in DET plot. The summary of the DET plot is described in Table 5-4.

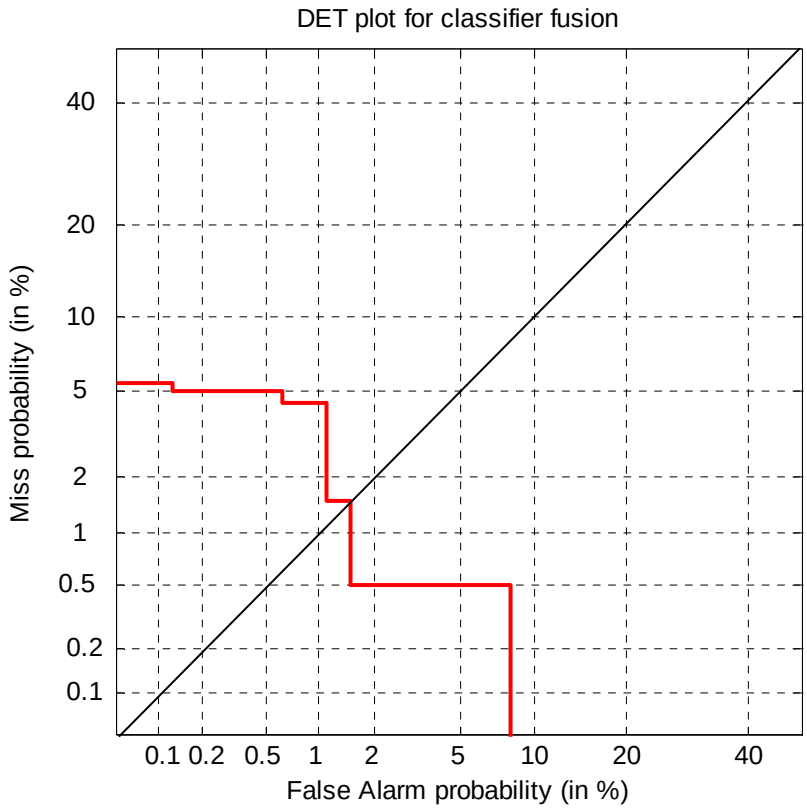

Figure 5.1 : DET plot for classification performance of good solder joints and defect solder joints

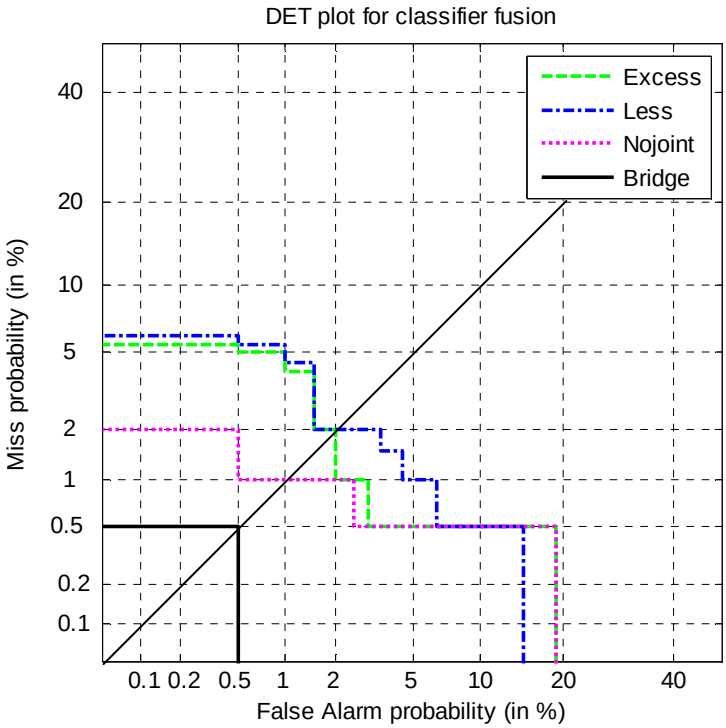

Figure 5.2 : DET plot for classification performance of good solder joints and individual defect solder joints

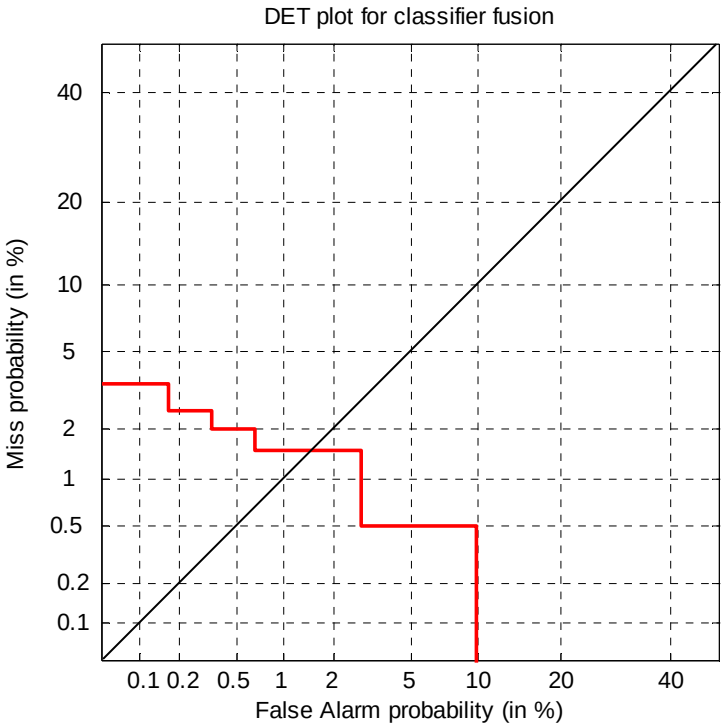

Figure 5.3 : DET plot for classification performance of excess solder joints and defect solder joints

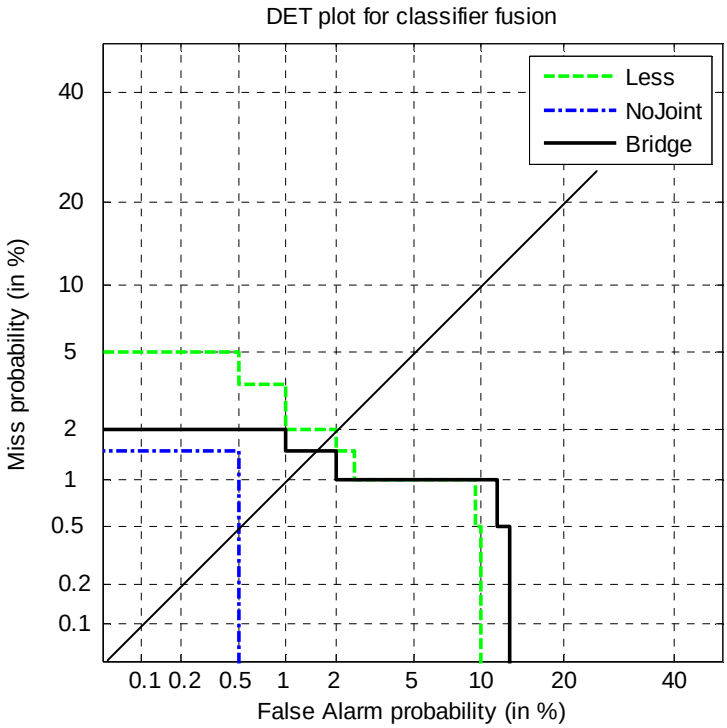

Figure 5.4 : DET plot for classification of performance of excess solder joints and other individual defect solder joints

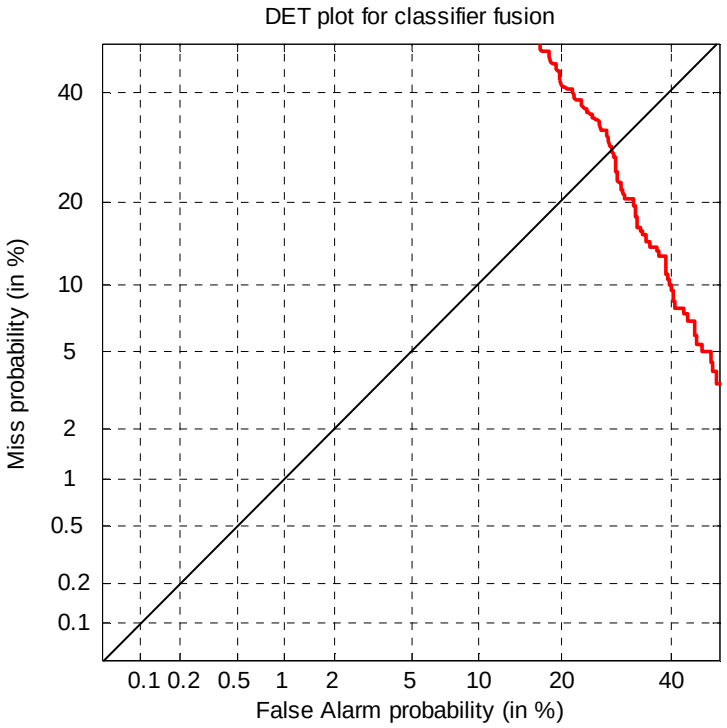

Figure 5.5 : DET plot for classification performance of less solder joints and defect solder joints

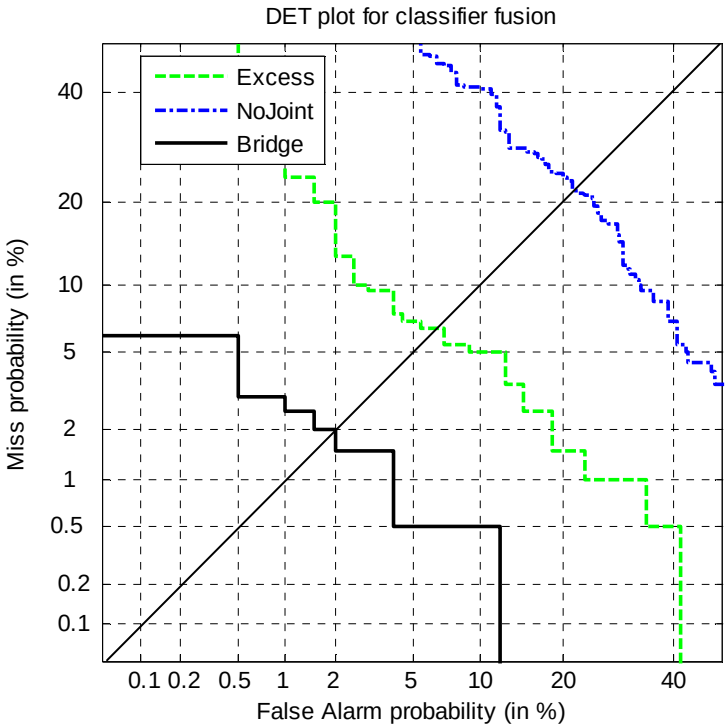

Figure 5.6 : DET plot for classification performance of less solder joints and other individual defect solder joints

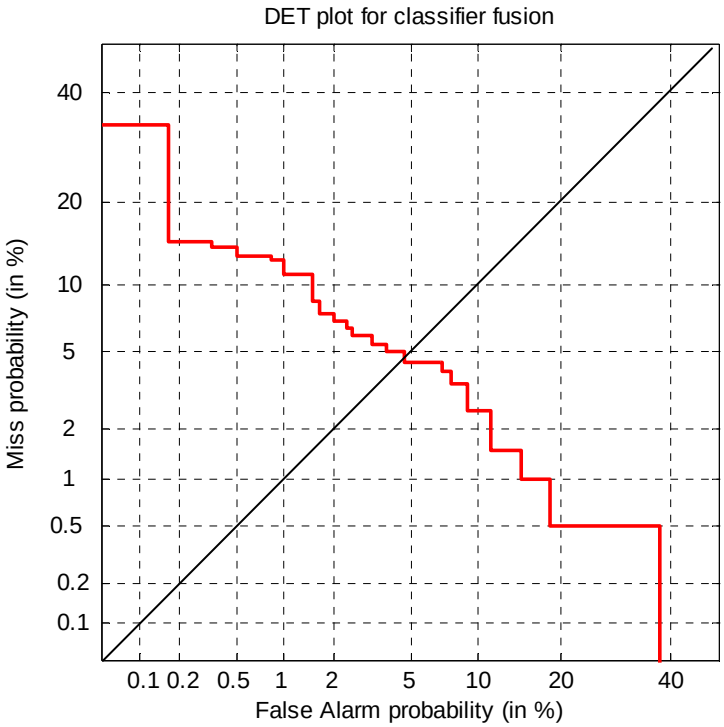

Figure 5.7 : DET plot for classification performance of no solder joints and defect joints

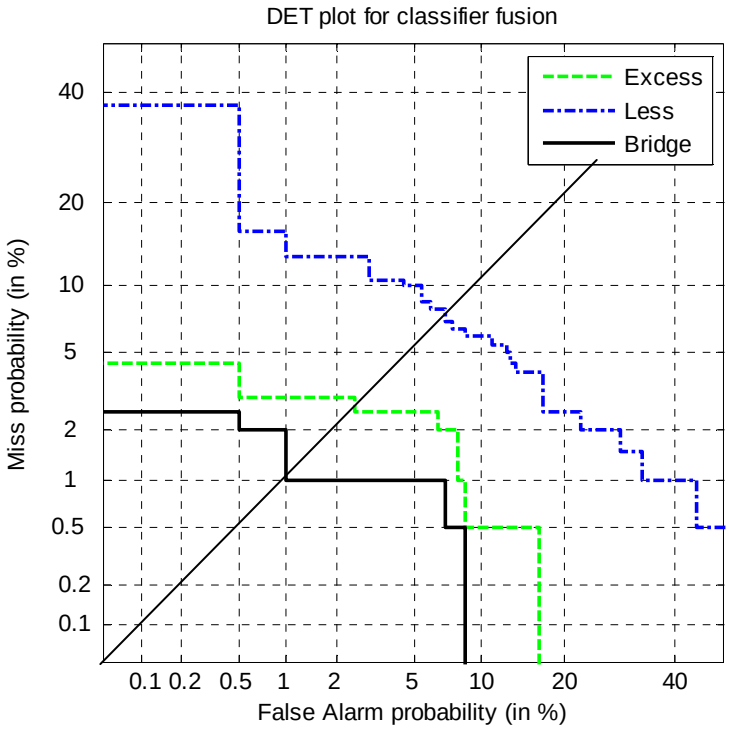

Figure 5.8 : DET plot for classification performance of no solder joints and other individual defect solder joints

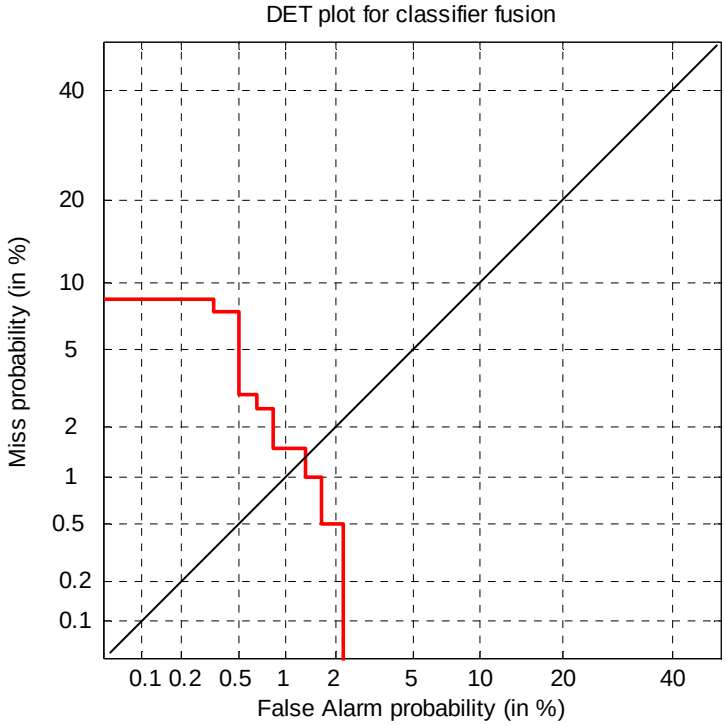

Figure 5.9 : DET plot for classification performance of bridge solder joints and defect solder joints

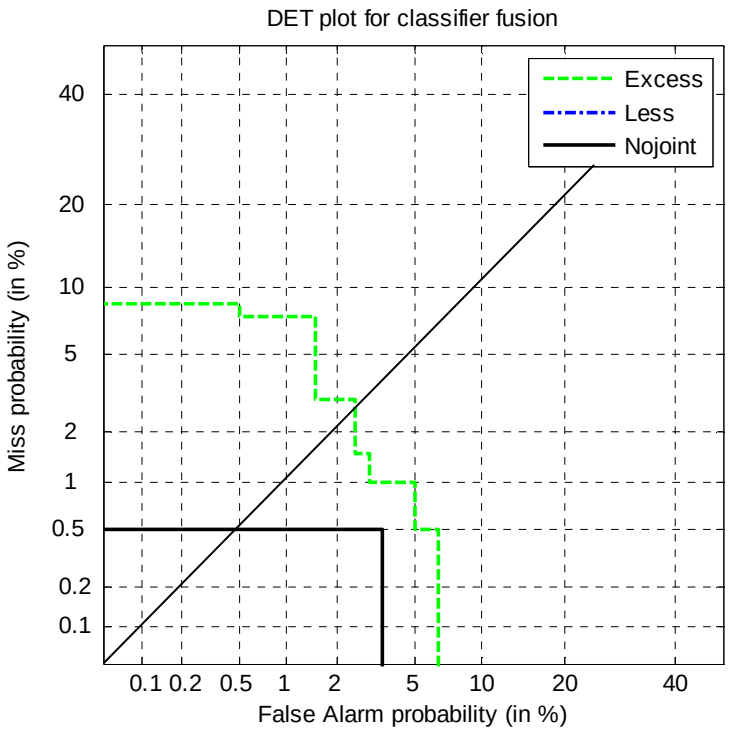

Figure 5.10: DET plot for classification performance of bridge solder joints and other individual defect solder joints

Since the overlap area between bridge solder joints and less solder joints is almost zero, it cannot be plotted on the DET and assumes that the EER is zero.

To demonstrate the recognition ability of this technique, the overall summary results of DET plots in the previous chapter are given from Table 5-1 to Table 5-3. Table 5-4 shows the recognition rate and EER for solder joint defect classification.

Solder Joint Types	Recognition rate and EER for Log Gabor filter				
	G	E	L	N	B
G (Good Joint)	**97**	3	4.5	1	0.5
E (Excess Joint)	-	**97**	2	4	1.5
L (Less Joint)	-	32	**60**	40	3.5
N (No Joint)	-	14	9	**90**	1
B (Bridge Joint)	-	7	0.5	0	**96.5**

Table 5-1 : Summary result for recognition rate of solder joints across five categories by using Log Gabor filter

Solder Joint Types	Recognition rate and EER for Wavelet Transform				
	G	E	L	N	B
G (Good Joint)	**96**	10.5	5	1.5	0.5
E (Excess Joint)	-	**86**	12	16	5
L (Less Joint)	-	20	**65**	>40	8
N (No Joint)	-	5	>40	**90**	16
B (Bridge Joint)	-	4	2	4	**96**

Table 5-2 : Summary result for recognition rate of solder joints across five categories by using Wavelet Transform

Solder Joint Types	Recognition rate and EER for Discrete Cosine Transform				
	G	E	L	N	B
G (Good Joint)	**95**	7	8	1	1
E (Excess Joint)	-	**93**	9	3	10
L (Less Joint)	-	>40	**<60**	40	33
N (No Joint)	-	>40	>40	**<60**	15
B (Bridge Joint)	-	7	1	1	**95**

Table 5-3 : Summary result for recognition rate of solder joints across five categories by using Discrete Cosine Transform

Solder Joint Types	Recognition rate and EER for Classifier Fusion				
	G	E	L	N	B
G (Good Joint)	**98.5**	2	2	1	0.5
E (Excess Joint)	-	**98.5**	2	0.5	1.5
L (Less Joint)	-	6.5	**70**	23	2
N (No Joint)	-	3	7	**95**	1
B (Bridge Joint)	-	3	0.5	0	**98.5**

Table 5-4 : Summary result for recognition rate of solder joints across five categories by using Classifier Fusion

It can be seen that the fusion of the Log Gabor filter, the Wavelet Transform and the Discrete Cosine Transform provides better performance than individual classifier. The correct classification rate of good solder joint, excess solder joint and bridge solder joint improves to 98.5% followed by classification rate of no solder joint which is 95% and that of less solder joint is increased from 60% to 70%.The average percentage of the correct classifications varies across different types from 98.5% to 70%. There are significant improvements in EER. Less than 5% of EER is achieved in most types of classification except for 6.5% of excess solder joint and 23% of no solder joint that are wrongly classified as less solder joint. 7% of less solder joint is wrongly classified as no solder joint.

It was anticipated that would lead to an improved classifier for classification of less solder joint, however, the results indicate that the linear fusion does not lead to improved classification. On the whole, a significant performance improvement is obtained. Scores from three classifiers (i.e., Log Gabor filter, DWT and DCT) fuse together to obtain the desired characteristics of the individual classifier. The main features of the individual filter are as follows. Log Gabor filters appear to be a logical choice for the task of frequency partitioning while wavelet analysis provides a compact representation which separates the frequency content of a signal or image. In addition, the Discrete Cosine Transform is associated with compression tasks and its compactness and similarities to the Fourier transform make it well suited to this research. Once more, the correct classification percentage is high for each type of the features mentioned above, and the features of Log Gabor filter achieve the highest percentage value. An advantage of the proposed approach is that this system does not need special positioning systems and the hardware for acquisition of the image. This allows less expensive solutions in the implementation of the classification system than those methods that require complex illumination systems.

5.3 Chapter Summary

In this chapter a general framework for fusion has been derived. This framework consists of a pre-processing where the scores are normalised using Z-score normalisation. This score normalisation may not lead to direct performance improvements but it provides a consistent frame of reference from which scores can

be examined and manipulated. The optimal weights for linear score fusion are derived by using the *llr* method.

The chapter demonstrates that the use of classifier fusion increases the information available for classification and greatly increases recognition performance. In deriving this linear classifier fusion in the solder joint defect classification, an important outcome is found. The system performance can be maintained if even one classifier fails because the linear classifier fusion is a form of the sum rule which is robust to estimation errors. In summary, work conducted in this chapter has led to the obvious improvement of solder joint defect classification system.

Chapter 6

Conclusions and Further Work

6.1 Conclusion

The attachment of electronic components to Print Circuit Boards (PCBs) has been accomplished generally by soldering technologies over the past few decades. Recently, with the development of new Surface Mount Technology (SMT), the need for automatic inspection is increasing. The current trends toward miniaturization of components, surface mounting technology, and highly automated assembly equipment make the task of detecting these defects more critical and more difficult.

In most applications, the detection of a fault is not enough to develop a completely automatic manufacturing system. It may be required to find the type of defect and to decide the reason for this defect. if it is important for the manufacturing process that may be responsible for the defect, then corrective action is in order. It can be clearly seen that detection of faults is not enough.

The research presented in this dissertation covers the development of an automated non-contact, non-destructive and low cost solder joint quality inspection system. It is also expected to be applicable to many types of surface mount devices such as chip resistors and capacitors and conventional lead frame packages, making it a versatile and cost-effective automated manufacturing tool. This tool could be used on-line as a go/on-go inspection tool, and off-line during process development for process optimization. Use of this solder joint defect inspection technology for automated manufacturing inspection will bring great cost savings by catching

defects early in the process. This could lead to reducing the time to market new products, and allowing better process optimization before manufacturing ramp-up.

6.2 Contribution of this Research

The three original contributions made in this thesis are:

(i) Improved solder joint segmentation by employing illumination normalisation

An illumination variation under different lighting conditions can be significantly reduced by using Discrete Cosine Transform. It can be easily implemented in a real-time recognition system by using this approach. The segmentation correctness achieves 99.93%.

(ii) Successful implementation of Log-Gabor filter bank in feature extraction of solder joint image

Log-Gabor filters are used as an optimal means of extracting feature from the solder joint images. These filters demonstrate the greater stability in the recognition of solder joint defects with overall classification rate of 97%. Analysis of the proposed method shows that Log-Gabor coefficients provide better overall performance than Discrete Cosine Transform and Discrete Wavelet Transform.

(iii) Improved solder joint defect classification by combining multiple algorithms.

A combination of three classifiers improves verification system through the fusion of the complementary information captured from multiple features. A weighted linear fusion using a Linear Logistic Regression (LLR) is successfully employed and achieves the classification rate of 98.5%. As illustrated in the experimental result, this method offers a potential approach for identification and classification of solder joint defects.

6.3 Future Work

The performance of the preliminary inspection algorithms is encouraging. While the classification correct reached 98%, there is still room for improvement. Some improvement can be expected to the current technologies.

- Select better feature to compute new individual features which are more representative of the solder joint classes and to compute combinations of features which provide even better class discrimination. By focusing on the errors of the current algorithm, some indication may be found that will lead to better features.

- Combinations of features may provide better performance than using one feature. In addition, experimentation with several different ways of combining features to get better features and compare their performance to the current algorithm.

- The Mahalanobis Cosine distance measure classifier is a simple classifier. There are many different kinds of classifiers which could be applied to this problem. More reliable decisions could be achieved by interaction of the input data with various production rules. Analysis of other different classification algorithm and selecting some of the more promising methods for implementation and testing them against the current algorithm.

- Some solder joint defects are not easily detected from directly over the PCBs board and cause only small changes at the surface. The use of multiple views of solder joints could improve classification performance and achieve more reliable inspection results.

- Certain parameters will usually change the performance of the algorithm. Further analysis should plan to investigate the effects of the following parameter changes. Check classification performance for different lens and different hardware (camera) device for same algorithm. Check classification accuracy for the same solder joints at different spatial resolutions to compute sensitivity to size changes.

Future work involves evaluation of the system in an actual production environment and development of a system for PCB manufacturing. Moreover, in the real world, many types of defective solder joint can be found in actual production PCB. Some other defects, such as overhang, high lead or no components, may need a different type of inspection system. Further research is required to develop a system that can detect such defects.

Bibliography

1. E. R. Davies, Automated Visual Inspection, Machine Vision, Second ed., Academic Press ed. New York, 1998.

2. J. L. C. Sanz and D. Petkovic, Machine vision algorithm for automated inspection of thin-film disk heads, IEEE Transactions on Pattern Analysis and Machine Intelligence, 10 (1988) 830-848.

3. C. Bahlmann, G. Heidemann and H. Ritter, Artificial neural networks for automated quality control of textile seams, Pattern Recognition, 32 (1999) 1049-1060.

4. H. Li and J. C. Lin, Using fuzzy logic to detect simple defects of polished wafer surfaces, IEEE Transactions on Industry Applications, 30 (1994) 1530-1543.

5. E. N. Malamas, E. G. M. Petrakis, M. Zervakis, L. Petit and J.-D. Legat, A survey on industrial vision systems, applications and tools, Image and Vision Computing, 21 (2003) 171-188.

6. M. Madhav, E. Fikret, H. D. Cihan and T. Shou, Automatic PCB inspection algorithms: a survey, 63 (1996) 287-313.

7. T. H. Kim, T. H. Cho, Y. S. Moon and S. H. Park, Visual inspection system for the classification of solder joints, Pattern Recognition, 32 (1999) 565-575.

8. S. L. Bartlett, P. J. Besl, C. L. Cole, R. Jain, D. Mukherjee and K. D. Skifstad, Automatic solder joint inspection, IEEE Transactions on Pattern Analysis and Machine Intelligence, 10 (1988) 31-43.

9. D. W. Capson and S. K. Eng, A tiered-color illumination approach for machine inspection of solder joints, IEEE Transactions on Pattern Analysis and Machine Intelligence, 10 (1988) 387-393.

10. S. Kobayashi, Y. Tanimura and T. Yotsuya, Apparatus for inspecting printed circuit boards and the like, and method of operating same. 1993: United States Patent No. 5,245,671.

11. J. S. Park, A reflectance model-based approach to highlight separation and surface description for inspection of 3 dimensional specular objects, University of Florida, 1991.

12. L. Zhang, Development of microelectronics solder joint inspection system: modal analysis, finite element modeling, and ultrasound signal processing, 2006.

13. N. S. S. Mar, C. Fookes and P. K. D. V. YarLagadda, Automatic solder joint defect classification using the Log-Gabor filter, Advanced Materials Research, 97-101 (2009) 2940-2943.

14. N. S. S. Mar, C. Fookes and P. K. D. V. YarLagadda, Automatic solder joint defect classification using the Log-Gabor filter, proceedings for the 3rd Smart Systems Postgraduate Student Conference (2009) 95-99.

15. A. N. Belbachir, M. Lera, A. Fanni and A. Montisci, An automatic optical inspection system for the diagnosis of printed circuits based on neural networks, Industry Applications Conference, 1 (2005) 680-684.

16. O. Oyeleye and E. A. Lehtihet, Automatic visual inspection of surface mount solder joint defects, International Journal of Production Research, 37 (1999) 1217-1242.

17. P. Kirippner and D. Beer, AOI Testing positions in comparison, Circuit Assembly, (2004) 26-32.

18. Y. Takagi, S. Hata and W. Beutel, Visual inspection machine for solder joints using tiered illumination, Machine Vision Systems Integration in Industry, 1386 (1990) 21-29.

19. J. H. Kim and H. S. Cho, Neural network-based inspection of solder joints using a circular illumination, Image and Vision Computing, 13 (1995) 479-490.

20. R. R. Lathrop, Jr., Solder paste print qualification using laser triangulation, IEEE Transactions on Components, Packaging and Manufacturing Technology, Part C, 20 (1997) 174-182.

21. Y. K. Ryu and H. S. Cho, A neural network approach to extended gaussian image based solder joint inspection, Mechatronics, 7 (1997) 159-184.

22. A. Khazan, Transducers and Their Elements: Design and Application Prentice Hall, 1994.

23. Y. Nakagawa, Y. Hara and M. Hashimoto, Automatic visual inspection using digital image processing, 34 (1985) 55-60.

24. J. H. Kim, H. S. Cho and S. Kim, Pattern classification of solder joint images using a correlation neural network, Engineering Applications of Artificial Intelligence, 9 (1996) 655-669.

25. S. N. Chiu and M. H. Perng, Reflection-area-based feature descriptor for solder joint inspection, Machine Vision and Applications, 18 (2007) 95-106.

26. H. H. Loh and M. S. Lu, Printed circuit board inspection using image analysis, IEEE Transactions on Industry Applications, 35 (1999) 426-432.

27. T. Ong, Z. Samad and M. Ratnam, Solder joint inspection with multi-angle imaging and an artificial neural network, The International Journal of Advanced Manufacturing Technology, 38 (2008) 455-462.

28. J. S. Park and J. T. Tou, A solder joint inspection system for automated printed circuit board manufacturing, IEEE International Conference on Robotics and Automation, 2 (1990) 1290-1295.

29. Z. S. Lee and L. R. Chin, Application of vision image cooperated with multi-light sources to recognition of solder joints for PCB, (2005).

30. K. W. Ko and H. S. Cho, Solder joints inspection using a neural network and fuzzy rule-based classification method, IEEE Transactions on Electronics Packaging Manufacturing, 23 (2000) 93-103.

31. G. Acciani, G. Brunetti and G. Fornarelli, Application of neural networks in optical inspection and classification of solder joints in surface mount technology, IEEE Transactions on Industrial Informatics, 2 (2006) 200-209.

32. G. Acciani, G. Brunetti and G. Fornarelli, A multiple neural network system to classify solder joints on integrated circuits, International Journal of Computational Intelligence Research, 2 (2006) 337-348.

33. L. Bing, Z. Yun, Y. Guangzhu and Z. Xianshan, ANN Ensembles Based Machine Vision Inspection for Solder Joints, IEEE International Conference on Control and Automation, (2007) 3111-3115.

34. T. S. Yun, Classification of Specular Object Based on Statistical Learning Theory, in Bio-Inspired Applications of Connectionism. 2001, 555-562.

35. T. S. Yun, K. J. Sim and H. J. Kim, Support vector machine-based inspection of solder joints using circular illumination, Electronics Letters, 36 (2000) 949-951.

36. B. C. Jiang, C. C. Wang and Y. N. Hsu, Machine vision and background remover-based approach for PCB solder joints inspection, 45 (2007) 451-464.

37. N. S. S. Mar, C. Fookes and P. K. D. V. YarLagadda, Design of automatic vision-based inspection system for solder joint segmentation, Achievements in Materials and Manufacturing Engineering, 34 (2009) 145-151.

38. MathWorks_Inc., Matlab; The language of technical computing.

39. R. C. Gonzalez, R. E. Woods and S. L. Eddins, Digital image processing using Matlab, First ed, Pearson Prentic Hall, 2004.

40. W. Chen, M. J. Er and S. Wu, Illumination compensation and normalization for robust face recognition using discrete cosine transform in logarithm domain, IEEE Transactions on Systems, Man, and Cybernetics-Part B, 36 (2006) 458-466.

41. A. A. Al-Nu'aimi and R. Qahwaji, Digital colored image watermarking using YIQ color format in discrete wavelet transform domain, 1-6.

42. T. W. Ridler and S. Calvard, Picture thresholding using an iterative selection method, IEEE Transactions on Systems, Man and Cybernetics, 8 (1978) 630-632.

43. Z. S. Lee and R. C. Lo, Application of vision image cooperated with multi-light sources to recognition of solder joints for PCB TAAI Artificial Intelligence and Applications, (2002) 425-430.

44. R. C. Gonzalez and R. E. Woods, Digital image processing, Second ed, Pearson Prentice Hall, 2002.

45. E. Frew, A. Huster and E. LeMaster, Image thresholding for object detection, 1997.

46. J. Cook, C. McCool, V. Chandran and S. Sridharan, Combined 2D/3D Face Recognition Using Log-Gabor Templates, IEEE International Conference on Video and Signal Based Surveillance, AVSS06 (2006) 83-83.

47. W. Y. Ma and B. S. Manjunath, Texture features and learning similarity, IEEE Computer Society Conference on Computer Vision and Pattern Recognition, (1996) 425-430.

48. T. Ying-li, T. Kanade and J. F. Cohn, Evaluation of Gabor-wavelet-based facial action unit recognition in image sequences of increasing complexity, Fifth IEEE International Conference on Automatic Face and Gesture Recognition, (2002) 229-234.

49. N. Rose, Facial Expression Classification using Gabor and Log-Gabor Filters, 7th International Conference on Automatic Face and Gesture Recognition, (2006) 346-350.

50. Z. Ying-Nan, J. Zhong, Y. Jing-Yu, L. Chuan-Cai and M. Xian-Quan, Practical Parameers Design for Gabor Filers with Application to Face Recognition, Machine Learning and Cybernetics, 2007 International Conference on, 4 (2007) 2229-2234.

51. Z. Yanfang, S. Nongliang, G. Yang and C. Maoyong, A new eye location method based on Ring Gabor Filter, IEEE International Conference on Automation and Logistics, (2008) 301-305.

52. H. Runping and Z. Lingmin, Fabric Defect Detection Method Based on Gabor Filter Mask, Global Congress on Intelligent Systems, 3 (2009) 184-188.

53. R. J. Nemati and M. Y. Javed, Fingerprint verification using filter-bank of Gabor and Log Gabor filters, Systems, Signals and Image Processing, 2008. IWSSIP 2008. 15th International Conference on, (2008) 363-366.

54. S. Zehang, G. Bebis and R. Miller, On-road vehicle detection using evolutionary Gabor filter optimization, IEEE Transactions on Intelligent Transportation Systems, 6 (2005) 125-137.

55. X. Sai-Cong, S. Nong-Liang and C. Mao-Yong, Wall-pasted cell segmentation based on circular Gabor filter bank, Wavelet Analysis and Pattern Recognition, 2007. ICWAPR '07. International Conference on, 4 (2007) 1735-1741.

56. W. M. Pan, C. Y. Suen and T. D. Bui, Script identification using steerable Gabor filters, Eighth International Conference on Document Analysis and Recognition, 2 (2005) 883-887.

57. K. R. Namuduri, R. Mehrotra and N. Ranganathan, Edge detection models based on Gabor filters, International Conference on Pattern Recognition Image, Speech and Signal Analysis, 3 (1992) 729-732.

58. C. Chia-Te, S. Sheng-Wen and C. Duan-Yu, Design of Gabor Filter Banks for Iris Recognition, Intelligent Information Hiding and Multimedia Signal Processing, 2006. IIH-MSP '06. International Conference on, (2006) 403-406.

59. Z. Ibrahim, S. A. R. Al-Attas, Z. Aspar and M. M. Mokji, Performance evaluation of wavelet-based PCB defect detection and localization algorithm, IEEE International Conference on Industrial Technology, 1 (2002) 226-231.

60. J. Daugman, Two-dimensional spectral analysis of cortical receptive field profiles, Vision Research, 20 (1980) 847-856.

61. A. E. Soohoo and T. R. Reed, Low-Bit-Rate coding of sequences using the Gabor transform, International Symposium and Exhibition, (1994) 641-644.

62. J. Cook, V. Chandran, S. Sridharan and C. Fookes, Gabor Filter Bank Representation for 3D Face Recognition, Digital Image Computing: Techniques and Applications, (2005) 16-23.

63. D. J. Field, Relations between the statistics of natural images and the response properties of cortical cells, Journal of Optical Society of America, 4 (1987) 2379-2394.

64. P. Kovesi, Invariant Measures of Image Features From Phase Information, The University of Western Australia, 1996.

65. M. Misiti, Y. Misiti, G. Oppenheim and J. M. Poggi, Wavelet Toolbox TM User's Guide The Math Works, Inc., 1997.

66. J. A. Cook, A Decompositional Investigation of 3D Face Recognition, Queensland University of Technology, Brisbane, Queensland, Australia, 2007.

67. S. Lucey and C. Tsuhan, Face recognition through mismatch driven representations of the face, 2nd Joint IEEE International Workshop on Visual Surveillance and Performance Evaluation of Tracking and Surveillance (2005) 193-199.

68. C. Sanderson and K. K. Paliwal, Fast features for face authentication under illumination direction changes, Pattern Recognition Letters, 24 (2003) 2409-2419.

69. S. Eickeler, S. Müller and G. Rigoll, Recognition of JPEG compressed face images based on statistical methods, Image and Vision Computing, 18 (2000) 279-287.

70. J. G. Daugman, Two-dimensional spectral analysis of cortical receptive field profiles, Vision Research, 20 (1980) 847-856.

71. V. S. Vyas and P. Rege, Automated texture analysis with gabor filter, GVIP Journal, 6 (2006).

72. M. Mokju and S. A. R. Abu-Bakar, Fingerprint matching based on directional image constructed using expanded Haar wavelet transform, International Conference on Computer Graphics, Imaging and Visualization, (2004) 149-152.

73. C. S. McCool, Hybrid 2D and 3D Face Verification, Queensland University of Technology, 2007.

74. N. Brummer, Tools for fusion and calibration of automatic speaker detection systems. Retrieved from http://www.dsp.sun.ac.za/.nbrummer/focal/index.htm.